Characterization of surface structure and p47 phox SH3 domain-mediated conformational changes for human neutrophil flavocytochrome b

ARTICLE · JANUARY 2007

CITATION
1

READS
8

1 AUTHOR:

Edgar Pick
Tel Aviv University
74 PUBLICATIONS **1,056** CITATIONS

SEE PROFILE

Characterization of Surface Structure and p47^{phox} SH3 Domain-Mediated Conformational Changes for Human Neutrophil Flavocytochrome *b*†

Ross M. Taylor,*,‡ Connie I. Lord,‡ Marcia H. Riesselman,‡ Jeannie M. Gripentrog,‡ Thomas L. Leto,§ Linda C. McPhail,|| Yevgeny Berdichevsky,⊥ Edgar Pick,⊥ and Algirdas J. Jesaitis‡

Department of Microbiology, 109 Lewis Hall, Montana State University, Bozeman, Montana 59717, Molecular Defenses Section, Laboratory of Host Defenses, National Institute of Allergy and Infectious Diseases, National Institutes of Health, Rockville, Maryland 20852, Department of Biochemistry, Wake Forest University, Medical Center Boulevard, Winston-Salem, North Carolina 27157, and Julius Friedrich Cohnheim-Minerva Center for Phagocyte Research and Ela Kodesz Institute of Host Defense against Infectious Diseases, Sackler School of Medicine, Tel Aviv University, Tel Aviv 69978, Israel

Received August 10, 2007; Revised Manuscript Received October 1, 2007

ABSTRACT: The heterodimeric, integral membrane protein flavocytochrome *b* (Cyt *b*) is the catalytic core of the phagocyte NADPH oxidase and generates superoxide which plays a critical role in host defense. To better define the activation of superoxide production by this multisubunit enzyme complex, Cyt *b*-specific monoclonal antibodies (mAbs) and the p47^{phox} SH3 domains (p47SH3$_{AB}$) were used in the present study as probes to map surface structure and conformational dynamics in human neutrophil Cyt *b*. In pull-down and co-immunoprecipitation studies with detergent-solubilized Cyt *b*, the oxidase-inhibitory mAb CS9 was shown to share an overlapping binding site with p47SH3$_{AB}$ on the C-terminal region of the p22^{phox} subunit. Similar studies demonstrated a surprising lack of overlap between the mAb 44.1 and CS9/p47SH3$_{AB}$ binding sites, and they indicated that the oxidase-inhibitory mAb NL7 binds a region physically separated from the p22^{phox} C-terminal domain. Resonance energy transfer and size exclusion chromatography confirmed the above results for functionally reconstituted Cyt *b* and provided evidence that binding of both mAb CS9 and p47SH3$_{AB}$ altered the conformation of Cyt *b*. Further support that binding of the p47^{phox} SH3 domains modulates the structure of Cyt *b* was obtained using a cell-free assay system where p47SH3$_{AB}$ enhanced superoxide production in the presence of a p67^{phox} (1−212)-Rac1(Q61L) fusion protein. Taken together, this study further characterizes the structure of human neutrophil Cyt *b* in both detergent micelles and reconstituted membrane bilayers, and it provides evidence that the cytosolic regulatory subunit p47^{phox} modulates the conformation of Cyt *b* (in addition to serving as an adapter protein) during oxidase activation.

Neutrophils represent the most abundant cell type of the innate immune system in humans and provide a first line of defense against a wide range of infectious agents. To carry out this essential host-defense function, the neutrophil can release an elaborate arsenal of microbicidal agents (including enzymes, antimicrobial peptides, and reactive oxygen species) that are designed to inhibit the spread of pathogenic organisms (*1*, *2*). Following activation by inflammatory stimuli, neutrophils are capable of generating high levels of superoxide and other reactive oxygen/nitrogen species (ROS/RNS[1]) that directly participate in microbial killing (*2*, *3*). Since ROS/RNS may not discriminate between pathogen and host at the molecular level, their production must be tightly regulated in order to minimize host tissue damage during a productive inflammatory response. In the vascular system, elevated superoxide production by phagocytic leukocytes has been observed in pathological conditions such as atherosclerosis (*4*), hypertension (*5*), and ischemia-reperfusion injury (*6*).

The main source of superoxide in activated neutrophils is a multisubunit NADPH oxidase complex (*3*). The oxidase is composed of the integral membrane protein flavocytochrome *b* (Cyt *b*) (*7*) and at least four cytosolic subunits (p40^{phox}, p47^{phox}, p67^{phox}, Rac1/2) (*8*−*10*), with the membrane and cytosolic components physically separated in unstimulated cells to prevent the unwanted generation of superoxide.

† This research was supported by American Heart Association Scientist Development Grant 0630253N (R.M.T.), the intramural research program of the National Institutes of Health, National Institute of Allergy and Infectious Diseases (T.L.L.), NIH R01 AI 22564 (L.C.M.), Israel Science Foundation Grant 19/05 and the Julius Friedrich Cohnheim - Minerva Center for Phagocyte Research (Y.B. and E.P.), and NIH RO1 AI 26711 (A.J.J).

* To whom correspondence should be addressed. Phone: (406) 994-4593. Fax: (406) 994-4926. E-mail: rosst@montana.edu.

‡ Montana State University.

§ National Institute of Allergy and Infectious Diseases.

|| Wake Forest University.

⊥ Sackler School of Medicine.

[1] Abbreviations: Ac, acetylated N-terminus of synthetic peptides; CCB, Cascade Blue; CNBr, cyanogen bromide; $CONH_2$, amidated C-terminus of synthetic peptides; Cyt *b*, human phagocyte flavocytochrome *b*; DDM, dodecylmaltoside; GST, glutathione *S*-transferase; IP, immunoprecipitation; IPTG, isopropyl-*β*-D-thiogalactopyranoside; mAb, monoclonal antibody; MALDI, matrix-assisted laser desorption/ionization; OG, octylglucoside; p47N, residues 1−286 of human p47^{phox}; p47SH3$_{AB}$, residues 151−286 of human p47^{phox}; PA, phosphatidic acid; PC, phosphatidylcholine; phox, phagocyte oxidase; RET, resonance energy transfer; RNS, reactive nitrogen species; ROS, reactive oxygen species.

10.1021/bi701626p CCC: $37.00
Published on Web 11/16/2007

In activated neutrophils, protein phosphorylation and lipid second messengers act at the level of both Cyt *b* (*11*, *12*) and the cytosolic oxidase regulatory subunits (*13*−*16*) to promote assembly of the catalytically active NADPH oxidase. Detailed investigation of the events that regulate superoxide production has suggested that p47^{phox} primarily serves a role in the oxidase assembly process, while Rac and/or p67^{phox} activate electron flow through Cyt *b* (*17*−*21*). The complexity of oxidase regulation is further highlighted by studies demonstrating that the small G-protein Rap1a (*22*), the arachidonate binding protein MRP8/ MRP14 (*23*), and the protein kinase Pak (*24*) can directly associate with Cyt *b* and that superoxide production is regulated by the segregation of individual oxidase components into specialized, cytoskeleton-enriched membrane microdomains (*25*−*27*).

The catalytic center of the NADPH oxidase complex is a heterodimeric, integral membrane protein (Cyt *b*) composed of a 570 residue large subunit (gp91^{phox}; Nox2) and a 195 residue small subunit (p22^{phox}) (*7*). The gp91^{phox} subunit contains the electron transport chain (including FAD and heme prosthetic groups) that shuttles electrons from NADPH to molecular oxygen (*28*−*30*), while the p22^{phox} subunit contains a well-characterized proline rich region recognized by p47^{phox} early in the oxidase assembly process (*31*−*33*). Spectroscopic methods have provided direct evidence that anionic lipids modulate the structure of Cyt *b* (*12*, *34*, *35*), which may serve an important regulatory function as the second messenger lipids arachidonic acid and phosphatidic acid promote superoxide production by the NADPH oxidase in intact cells (*36*, *37*). Although binding of the cytosolic regulatory subunits to Cyt *b* is also generally assumed to induce conformational changes that activate superoxide production (*17*, *38*, *39*), difficulties associated with direct structure analysis of Cyt *b* have hindered a detailed molecular understanding of the consequences of oxidase assembly.

Monoclonal antibodies (mAbs) that recognize the gp91^{phox} and p22^{phox} subunits of Cyt *b* have provided valuable reagents for the analysis of Cyt *b* structure (*40*−*43*) and conformational dynamics (*12*). Additionally, mAbs that bind Cyt *b* and inhibit superoxide production (*42*−*44*) are of interest as they likely target distinct steps of the oxidase activation process and represent potential therapeutic agents. In the present study, a panel of Cyt *b*-specific mAbs and the p47^{phox} tandem SH3 domains (p47SH3$_{AB}$) were used as site-specific structural probes in order to better define the initial stages of assembly and activation of the NADPH oxidase complex. Using human neutrophil membrane extracts as the source of Cyt *b*, pull-down and co-immunoprecipitation studies demonstrated that the oxidase-inhibitory mAb CS9 selectively disrupts binding of p47SH3$_{AB}$ to Cyt *b*. In support of these results, MALDI mass spectrometry and peptide inhibition studies were used to confidently localize the mAb CS9 core epitope to a region adjacent to the p47SH3$_{AB}$ binding site on the C-terminal domain of p22^{phox}. In addition to studies conducted with detergent-solubilized Cyt *b*, the high sensitivity and binding specificity afforded by fluorescent mAb conjugates enabled surface structure mapping of functionally reconstituted Cyt *b* by both resonance energy transfer and size exclusion chromatography, representing the first studies of this nature carried out for Cyt *b* in the context of the lipid bilayer. Using both detergent-solubilized and reconstituted Cyt *b*, evidence was obtained that binding of the p47^{phox} tandem SH3 domains induces conformational changes in Cyt *b*. The potential relevance of p47^{phox} SH3 domain-induced conformational changes was supported by the previously unreported ability of p47SH3$_{AB}$ to markedly enhance the activation of Cyt *b* in cell-free superoxide production assays.

EXPERIMENTAL PROCEDURES

Materials. The expression vector pGex4T-1 was from GE Biosciences (Piscataway, NJ); the expression vector pET-30a and the *E. coli* expression strain BL21(DE3)pLysS were from Novagen (Madison, WI); and the nickel NTA-Agarose beads were from Qiagen (Valencia, CA). The anti-GST monoclonal antibody was from GenScript (Piscataway, NJ); the Zorbax GF-250 size exclusion column was from Agilent (Santa Clara, CA); and the peptide Ac-AEARKKPSEEEAA-$CONH_2$ was obtained from Global Peptides (Fort Collins, CO). The QuickChange II-E site-directed mutagenesis kit was obtained from Stratagene (La Jolla, CA). All other reagents were obtained from Sigma-Aldrich (St. Louis, MO) or have been described in previous reports by our group (*12*, *43*, *45*, *46*). The instrumentation used for absorption spectroscopy, MALDI mass spectrometry, resonance energy transfer, chromatographic analysis, and superoxide production assays has also been described in the above studies.

Recombinant Cytosolic Oxidase Subunits. For the generation of GST-p47^{phox} fusion proteins, residues 1−286 and 151−286 of human p47^{phox} (*32*, *33*, *47*) were amplified by PCR, cloned into the EcoRI/NotI sites of pGex4T-1 (GE Biosciences), and verified by DNA sequence analysis. For expression, constructs were transformed into *E. coli* BL21-(DE3)pLysS (Novagen), and protein expression was induced with 0.1 mM IPTG (Promega) for 3 h at 25 °C following cell growth. Cells were then harvested by centrifugation and the resulting cell pellets stored at −20 °C. For purification, frozen pellets from 1 L of cells were resuspended by homogenization in 20 mL of 50 mM Hepes (pH 8.0)/200 mM NaCl (Buffer A), containing 100 μg/mL deoxyribonuclease I (bovine pancreas; Sigma-Aldrich), 100 μg/mL ribonuclease B (bovine pancreas; Sigma-Aldrich), 100 μg/mL lysozyme (chicken egg white; Sigma-Aldrich), 2 mM PMSF (CalBiochem), 1 μL/mL protease inhibitor cocktail (catalog P8340; Sigma-Aldrich), and then stirred on ice for 5 min. Following brief probe sonication, cells were brought to 1% Triton X-100 (Sigma-Aldrich) and stirred on ice for an additional 15 min. Centrifugation was then conducted (30 000*g* for 30 min at 4 °C) to remove insoluble material, and the resulting cell extract was rotated with 2.5 mL of glutathione-Agarose (Sigma-Aldrich) for 1 h at 4 °C. Following this incubation, unbound material removed by washing with Buffer A until the absorbance (200−700 nm) of the column flow fraction was at baseline. The GST-p47^{phox} constructs were then eluted by rotating the beads with Buffer A/10 mM reduced glutathione (Sigma-Aldrich) for 10 min at 4 °C, and the resulting material was extensively dialyzed against PBS at 4 °C. Following dialysis, fractions containing fusion proteins were concentrated using an Amicon 5000 molecular weight cutoff concentrator (Millipore), adjusted to 20% glycerol (EMD Biosciences), and stored at −20 °C. Protein concentration was determined by absorption spectroscopy with extinction coefficients calculated from primary

sequence using the program ProtParam (http://ca.expasy.org/tools/#primary).

For the preparation of p47^{phox} 1−286 (p47N) and p47^{phox} 151−286 (p47SH3$_{AB}$), 0.5 mg of the GST fusion protein was digested with 10 units of thrombin (bovine plasma; Sigma-Aldrich) for 3 h at room temperature. Thrombin digests were terminated with 2 mM PMSF, and the reactions were centrifuged at 100 000*g* for 20 min. The digests were then rotated with ∼80 μL of glutathione-Agarose beads for 2 h at 4 °C for removal of both GST and uncleaved fusion protein.

The construct encoding the His-tagged p67^{phox} (1−212)-Rac1(Q61L) fusion protein was generated by ligation into the BamHI/EcoRI sites of a modified pET-30a vector (Novagen) resulting in the following construct starting at the NdeI site: Met-6His-Gly-Ser-Met-p67^{phox} (1−212)-Rac1-(Q61L). For expression, this construct was transformed into *E. coli* BL21-CodonPlus (DE3)-RIL (Stratagene) and induced with 100 μM IPTG for 18 h at 16 °C. For purification, cells were processed as described above, with the exception that (1) the p67^{phox} (1−212)-Rac1(Q61L) fusion protein was bound to nickel NTA-Agarose beads (Qiagen); (2) the column was washed with Buffer A and then Buffer A/15 mM imidazole (Sigma-Aldrich); and (3) the elution was carried out with Buffer A/300 mM imidazole. Following elution, the p67^{phox} (1−212)-Rac1(Q61L) fusion protein was processed and stored as described above.

The W193R mutation was introduced into GST-p475H3$_{AB}$ using the QuickChange II-E site-directed mutagenesis kit (Stratagene) according to the manufacturer's instructions using the following primers: 5′ mutagenesis primer, GAGAA-GAGCGAGAGCGGTAGGTGGTTCTGTCAGATG; 3′ mutagenesis primer, 5′ CATCTGACAGAACCACCTACCGCT-CTCGCTCTTCTC. The GST-p67^{phox} (1−212)-Rac1 and GST-p47^{phox} fusion proteins that were also used in this study have been previously described (*32*, *48*).

Coupling of mAbs to CNBr-Sepharose. Prior to coupling of antibody, CNBr-Sepharose beads (GE Biosciences) were prepared according to the manufacturer's instructions. For coupling, 2 mg of mAb was diluted into 100 mM $NaHCO_3$/500 mM NaCl (7.5 mL total volume) and rotated with 1 mL of CNBr-Sepharose for 30 min at room temperature. Following this incubation, beads were washed with 5 volumes of 100 mM $NaHCO_3$/500 mM NaCl and then blocked with 100 mM Tris (pH 8.0)/500 mM NaCl for 1 h at room temperature. Antibody beads were then washed with PBS/0.02% NaN_3 and stored at 4 °C.

Extraction of Neutrophil Membranes. To generate detergent-solubilized Cyt *b* for binding studies, 1 mL of neutrophil membranes (5×10^8 cell equivalents/mL) was extracted with 0.8% dodecylmaltoside (DDM) (Anatrace) as described (*45*), with the exception that extractions were conducted at 4 °C using 2 mL total of extraction buffer. Following centrifugation at 100 000*g* for 30 min, detergent extracts were diluted 2-fold in 10 mM Hepes (pH 7.4)/100 mM KCl/10 mM NaCl/1 mM EDTA (Buffer B) on ice. The final diluted neutrophil membrane extracts contained ∼40−90 nM Cyt *b* based on heme absorption.

Analysis of Surface Structure Using Detergent-Solubilized Cyt b. For pull-down assays, glutathione-Agarose beads were loaded with GST, GST-p47N, GST-p47SH3$_{AB}$, or GST-p47SH3$_{AB}$(W193R) at a final concentration of 20 pmol protein/μL beads. To analyze binding interactions, 300 μL of the neutrophil membrane extract were rotated with ∼40 μL of loaded glutathione beads for 2 h at 4 °C. Following incubation, the beads were washed 3 × 5 min at 4 °C with Buffer B/0.1% DDM and then eluted with 300 μL of PBS/1% SDS (Sigma-Aldrich) for 10 min at room temperature. In some studies, Cyt *b*-specific mAbs (1 μM final) were preincubated with neutrophil membrane extracts for 20 min on ice prior to incubation of extracts with the loaded glutathione beads. To detect binding, samples were resolved by SDS-PAGE using either 12.5% continuous or 5−20% gradient gels, and then they were transferred to nitrocellulose (Schleicher & Schuell) for immunoblot analysis of the p22^{phox} subunit using mAb CS9 (*43*) and the gp91^{phox} subunit using mAb 54.1 (*40*).

To analyze binding interactions by co-immunoprecipitation (co-IP), neutrophil membrane extracts were incubated with PBS, GST-p47N, GST-p47SH3$_{AB}$, or GST-p47SH3$_{AB}$-(W193R) (1 μM final GST and GST fusion proteins) for 20 min on ice. The above mixtures (300 μL) were then rotated with ∼40 μL of mAb-Sepharose beads (13 pmol mAb/μl beads) for 2 h at 4 °C. Following this incubation, reactions were processed as described above for pull-down assays, with immunoblot analysis subsequently carried out for both p22^{phox} (using mAb CS9) and the GST component of the p47^{phox} constructs.

Immunoaffinity Purification of Cyt b. Affinity purification was conducted as described (*45*, *46*), with Cyt *b* stored at −20 °C prior to use.

Physical Mapping of the mAb CS9 Epitope. For analysis by MALDI mass spectrometry, 40 μL of purified Cyt *b* (10 pmol) was incubated with 15 μL of mAb CS9-Sepharose (195 pmol CS9) overnight at room temperature. Following this incubation, the supernatant fraction was removed and the beads were washed with 400 μL of 20 mM NH_4HCO_3/0.1% DDM. The beads were then resuspended in 50 μL of 20 mM NH_4HCO_3/0.1% DDM and digested with 10 ng of trypsin (mass spectrometry grade; Promega) for 7 h at room temperature with the beads pipetted every hour to facilitate mixing. Following digestion, the supernatant fraction was removed and the beads were washed with 400 μL of 20 mM NH_4HCO_3/0.1% DDM, followed by 400 μL of 20 mM NH_4HCO_3. Tryptic peptides bound to the mAb CS9-Sepharose were then eluted with 100 μL of 50% acetonitrile/0.1% trifluoroacetic acid (both from J.T. Baker). The elution fraction was dried by vacuum centrifugation and resuspended in 10 μL of 50% acetonitrile/0.1% trifluoroacetic acid for MALDI mass spectrometry as described (*46*).

To fine map the mAb CS9 epitope, the effect of synthetic peptides on the mAb CS9:Cyt *b* interaction was examined in IP studies. Epitope-mimicking peptides for mAbs 44.1 (Ac-PQVRPI-$CONH_2$) (Macromolecular Resources; Fort Collins, CO) and CS9 (Ac-AEARKKPSEEEAA-$CONH_2$) (Global peptides; Fort Collins, CO) were dissolved at 10 mM in distilled water and stored at −20 °C prior to use. To evaluate the effect of peptides, IP reactions were incubated as described above for 1.5 h at 4 °C, at which point PBS, the mAb CS9 epitope-mimicking peptide, or the irrelevant mAb 44.1 epitope-mimicking peptide were added directly to the reaction (200 μM peptide final). The resulting mixtures were rotated for an additional 30 min at 4 °C and then

processed as for immunoblot analysis of $p22^{phox}$ using mAb CS9.

Functional Reconstitution of Cyt b. The generation of functionally active Cyt *b* was carried out by reconstitution of partially purified Cyt *b* as follows. For partial purification, 10 mL of neutrophil membrane fractions (5×10^9 total cell equivalents) were extracted as previously described (*45*), with the exception that all steps were carried out at 4 °C. The resulting extract was diluted 7-fold into 10 mM Hepes (pH 7.4) and rotated with 1 mL of heparin-Sepharose (GE Biosciences) for 1 h at 4 °C to allow binding. The matrix was then washed with 10 mM Hepes (pH 7.4)/20 mM NaCl/1.2% octylglucoside (OG) (CalBiochem) to remove unbound proteins and exchange detergent. Bound material was eluted from the heparin matrix with 10 mM Hepes (pH 7.4)/800 mM NaCl/1.2% OG, with the resulting Cyt *b*-containing fractions detected by absorption spectroscopy and pooled.

Functional reconstitution was carried out by dialysis as described (*49*) using 99% phosphatidylcholine (PC) (Type XVI-E; Sigma-Aldrich) at a final concentration of 200 μg/mL. Following dialysis, the resulting proteoliposomes were stored at −80 °C prior to use. Analysis of the reconstitution mixtures by absorption spectroscopy (200−700 nm) revealed variable degrees of optical turbidity (light scattering), which was largely removed by centrifugation at 12 000*g* for 2 min. Importantly, NADPH oxidase activity (a measure of functional Cyt *b*) was equivalent in samples before and after centrifugation, and clarified proteoliposomes (containing ∼700−950 nM Cyt *b* based on absorption spectroscopy) were used throughout the present study.

Preparation of mAb Conjugates. Labeling of mAbs 44.1 and CS9 with Cascade Blue (CCB) acetyl azide (Molecular Probes) was carried out as previously described (*12*), using the room temperature protocol. After desalting on the P10 column (Bio-Rad), labeled mAbs were concentrated to ∼250 μL using an Amicon 50 000 molecular weight cutoff concentrator (Millipore) and subject to a final purification using a Zorbax-250 gel filtration column (Agilent) run in PBS at 1 mL/min. The CCB-44.1 and CCB-CS9 stocks used in this study were calculated to have a labeling stoichiometry of 4−5:1 (CCB:mAb molar ratio) and were stored at 4 °C prior to use.

Resonance Energy Transfer. RET experiments were conducted as described (*12*), with the following modifications. The anionic lipid 10:0 phosphatidic acid (PA) (Avanti Polar Lipids) was prepared as a 1.5 mM stock in distilled water and stored at −20 °C. To prepare the RET working solutions, CCB-labeled mAb (21 nM mAb final) and mAb K16 (irrelevant mAb; 667 nM final) were diluted into PBS and filtered (working solutions were stored at 4 °C and equilibrated to room temperature prior to RET analysis). Prior to measurements, 15 μL of Cyt *b*-containing proteoliposomes were incubated with 15 μL of the agents under investigation (PBS, GST, GST-p47N, GST-p47SH3$_{AB}$, GST-p47SH3$_{AB}$-(W193R) (21 μM stocks of GST and GST fusion proteins), or unlabeled mAb (13 μM stocks)) for 15 min at room temperature. For RET studies, the fluorescence emission of CCB-CS9 or CCB-44.1 (470 μL total) was monitored for 1 min prior to the addition of Cyt *b*-containing proteoliposomes (30 μL total) treated as outlined above. For some studies with CCB-CS9, the anionic lipid 10:0 PA was included in both the Cyt *b* preincubation (50 μM PA) and the CCB-CS9 working solution (10 μM PA). In all cases, control experiments were conducted to ensure that the various agents under investigation did not alter the fluorescence emission of CCB-44.1 and CCB-CS9 in the absence of Cyt *b*.

Size Exclusion Chromatography. For size exclusion studies, 15 μL of Cyt *b*-containing proteoliposomes was incubated with 15 μL of the agents under investigation (as described for RET experiments) for 15 min at room temperature. The CCB-CS9 or CCB-44.1 working solutions (220 μL) described for RET were then added to Cyt *b* and incubated for 15 min at room temperature. The resulting mixtures (250 μL total volume) were then analyzed on a Superdex 200 size exclusion column (GE Biosciences) (run in PBS at 0.7 mL/min), with CCB-mAbs detected by monitoring CCB fluorescence (λ_{ex} 376 nm and λ_{em} 425 nm). In these studies, it was absolutely critical to presaturate the column with PC vesicles (99% PC prepared at 1 mg/mL by dialysis) for efficient recovery of proteoliposomes (*50*), and several chromatographic runs were required before maximum, stable recoveries were achieved. For quantitation, the relative signal intensities of vesicle-associated and free CCB-mAb were evaluated by integration of the respective chromatographic peaks. In all cases, control experiments were conducted to ensure that various agents under investigation did not alter the chromatographic profiles of CCB-44.1 and CCB-CS9 in the absence of Cyt *b*.

Cell-Free Superoxide Production Assays. Cell-free assays were conducted as previously described (*43*), using both isolated neutrophil membrane fractions and 99% PC proteoliposomes as the source of Cyt *b*. In studies analyzing the effects of the $p47^{phox}$ SH3 domains on activation of superoxide production by $p67^{phox}$ (1−212)-Rac1 fusion proteins, individual reaction wells contained (1) 10:0 PA as the anionic lipid activator (80 μM final); (2) His-tagged $p67^{phox}$ (1−212)-Rac1(Q61L) or GST-$p67^{phox}$ (1−212)-Rac1 as the source of cytosolic oxidase subunits (0−960 nM final in 2-fold increasing concentrations); (3) a presence or absence of p47N or p47SH3$_{AB}$ (400 nM final); and (4) 200 μM final NADPH to initiate superoxide production. The assay system described above was used to evaluate the effect of the W193R mutation on the potentiation of superoxide production by p47SH3$_{AB}$ (using neutrophil membranes), with the exception that individual reaction wells contained (1) His-tagged $p67^{phox}$ (1−212)-Rac1(Q61L) (200 nM final) and (2) GST-$p47^{phox}$, GST-p47SH3$_{AB}$, or GST-p47SH3$_{AB}$(W193R) (200 nM final GST fusion proteins). For studies with $p67^{phox}$ (1−212)-Rac1 fusion proteins, the constructs were used without nucleotide exchange to the GTP-bound form. For all cell-free assay studies, the lipid activator 10:0 PA and $p67^{phox}$ (1−212)-Rac1 fusion proteins were absolutely required for high rates of superoxide production.

Statistical Analysis. Statistical analysis was performed with Graphpad Prism (Version 3.03) and Microsoft Excel. Data are presented as mean ± standard deviation, and a two-tailed Student's *t* test was used to determine *P* values. A *P* value of ≤0.05 was taken to represent a significant difference where indicated for densitometric analysis, RET analysis, and superoxide production assays. Since certain conditions were arbitrarily set to 100% in some assays for internal comparisons (mAb 7D5-Sepharose in co-IP studies and PBS treatment in RET studies), the maximum error observed for

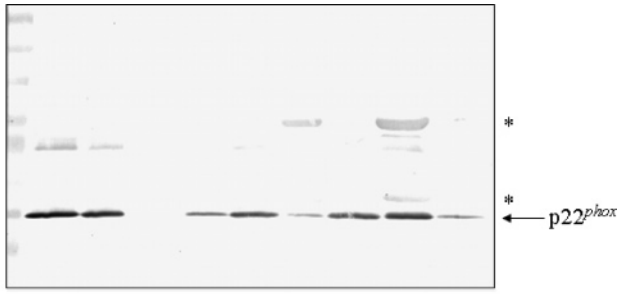

FIGURE 1: Oxidase-inhibitory mAb CS9 specifically disrupts binding of the p47*phox* SH3 domains to Cyt *b*. Following solubilization of human neutrophil membranes, extracts were incubated with glutathione-Agarose beads loaded with GST or GST-p47N. To detect binding, the indicated fractions were analyzed for Cyt *b* content by immunoblot probing the p22*phox* subunit. In some cases, extracts were incubated with mAb CS9 or the irrelevant mAb K16 prior to incubation with beads. Lane 1, DDM extract (total Cyt *b*); lane 2, GST supernatant; lane 3, GST beads; lane 4, GST-p47N supernatant; lane 5, GST-p47N beads; lane 6, GST-p47N supernatant, mAb K16 preincubation; lane 7, GST-p47N beads, mAb K16 preincubation; lane 8, GST-p47N supernatant, mAb CS9 preincubation; lane 9, GST-p47N beads, mAb CS9 preincubation. Asterisks (*) show the mAb heavy and light chains detected by the anti-mouse secondary antibody.

Table 1: Cyt *b* Structural Probes Used in This Study

probe	core binding determinant	refs
p47N and p47SH3$_{AB}$	p22*phox* residues 151−164	*32*, *33*, *51*, *52*
mAb 7D5	gp91*phox* residues 160−163 and 226−230	*53*
mAb CS9	p22*phox* residues 165−169	*43*
mAb 44.1	p22*phox* residues 29−33 and 182−188	*41*
mAb NL7	gp91*phox* residues 498−507	*44*

any other condition in the assay system was assigned to the above samples for the determination of *P* values.

RESULTS

Mapping the p47phox Binding Site on Human Neutrophil Flavocytochrome b Using Cyt b-Specific mAbs. Monoclonal antibody CS9 binds the p22*phox* subunit of human neutrophil Cyt *b* and inhibits superoxide production by the NADPH oxidase complex in cell-free assays (*43*). Phage display epitope mapping has proposed a core CS9 epitope that is located near a proline rich region on the cytosolic, C-terminal tail of p22*phox* (*43*) that serves as a critical p47*phox* binding site (*32*, *33*, *51*, *52*) (Table 1).

In order to test the hypothesis that mAb CS9 inhibits superoxide production (at least in part) by disrupting oxidase assembly, methods were developed to examine the ability of mAb CS9 to disrupt binding of recombinant p47*phox* fragments to intact, detergent-solubilized Cyt *b*. For initial binding studies, glutathione-Agarose beads were loaded with GST alone, GST-p47N (p47*phox* PX and tandem SH3 domains), or GST-p47SH3$_{AB}$ (p47*phox* tandem SH3 domains) for use in pull-down assays with neutrophil membrane extracts used as the source of Cyt *b* (approximately 2700 nM GST or GST fusion protein and 40−90 nM Cyt *b* final). As shown in Figure 1, while glutathione beads containing GST alone had no observable interaction with Cyt *b* (lanes 2 and 3), beads loaded with GST-p47N efficiently bound to Cyt *b* present in the membrane extracts (lanes 4 and 5). To evaluate the spatial proximity of the mAb CS9 and p47*phox* binding sites, neutrophil membrane extracts were preincubated with mAb K16 (isotype-matched, irrelevant antibody) or mAb CS9 prior to incubation with the loaded beads (1000 nM mAb final). In these studies, preincubation of membrane extracts with mAb K16 had no measurable effect on the binding of GST-p47N to Cyt *b* (Figure 1, lanes 6 and 7), while mAb CS9 effectively disrupted this binding interaction (Figure 1, lanes 8 and 9).

To provide a more comprehensive analysis of the p47*phox* binding site, additional epitope-mapped mAbs that bind the gp91*phox* and p22*phox* subunits of Cyt *b* (Table 1 and Figure 8) were also examined for the ability to disrupt binding of GST-p47N and GST-p47SH3$_{AB}$. Since the relative affinities of the various binding interactions have not been determined, co-IP studies were used to measure the ability of mAbs to simultaneously occupy the surface of Cyt *b* with the p47*phox* constructs. For co-IP studies, neutrophil membrane extracts were first incubated with GST-p47N or GST-p47SH3$_{AB}$ to allow binding to Cyt *b*, and the resulting mixtures were then precipitated using mAb-Sepharose beads that bound distinct regions of Cyt *b* (approximately 40−90 nM Cyt *b*/1000 nM p47*phox* constructs, and 1733 nM mAb final). As shown in Figure 2A,B, the recombinant p47*phox* constructs were efficiently co-immunoprecipitated with Cyt *b* by a mAb 7D5 affinity matrix. Since 7D5 binds an extracellular epitope on Cyt *b* (*53*) that is topologically distinct from the p47*phox* binding site, these results would be anticipated and demonstrate the utility of this method for detecting binding of the p47*phox* constructs to intact Cyt *b*. In co-IP studies using 44.1-Sepharose (*41*) and NL7-Sepharose (*44*), binding of the recombinant p47*phox* constructs was similar to that observed with mAb 7D5 (Figure 2A,B). In contrast to the above results, immunoprecipitation of Cyt *b* with mAb CS9-Sepharose beads markedly disrupted binding of both GST-p47N and GST-p47SH3$_{AB}$ (Figure 2A,B). Importantly, control experiments showed no detectable binding of GST-p47N and GST-p47SH3$_{AB}$ by the mAb affinity matrices in the absence of Cyt *b* and no measurable binding of Cyt *b* to K16-Sepharose beads, confirming the specificity of this assay system (data not shown). In addition, control experiments using GST-p47SH3$_{AB}$(W193R) (containing a point mutation that disrupts the binding of p47*phox*) (*54*) showed no measurable binding to detergent-solubilized Cyt *b* when this construct was loaded on glutathione beads (Figure 2C, lanes 1−4) or used in co-IP experiments (Figure 2C, lanes 5−7). Taken together, the above studies support the hypothesis that the binding sites for mAb CS9 and the p47*phox* SH3 domains physically overlap on Cyt *b* (as defined by the structural probes used in these studies). The ability of both mAb 44.1 and mAb NL7 to co-IP levels of p47N and p47SH3$_{AB}$ that are similar to mAb 7D5 indicates that these mAbs bind epitopes that do not spatially overlap with the p47*phox* SH3 domain binding site (results summarized in Table 2).

Biochemical Characterization of the mAb CS9 Epitope. Since mAb CS9 uniquely disrupted binding of the p47*phox* SH3 domains to Cyt *b*, the mAb CS9 core epitope was directly determined to allow for confident interpretation of binding studies. For initial mapping, purified Cyt *b* was bound to mAb CS9-Sepharose, digested by trypsin, and then analyzed by mass spectrometry for identification of tryptic

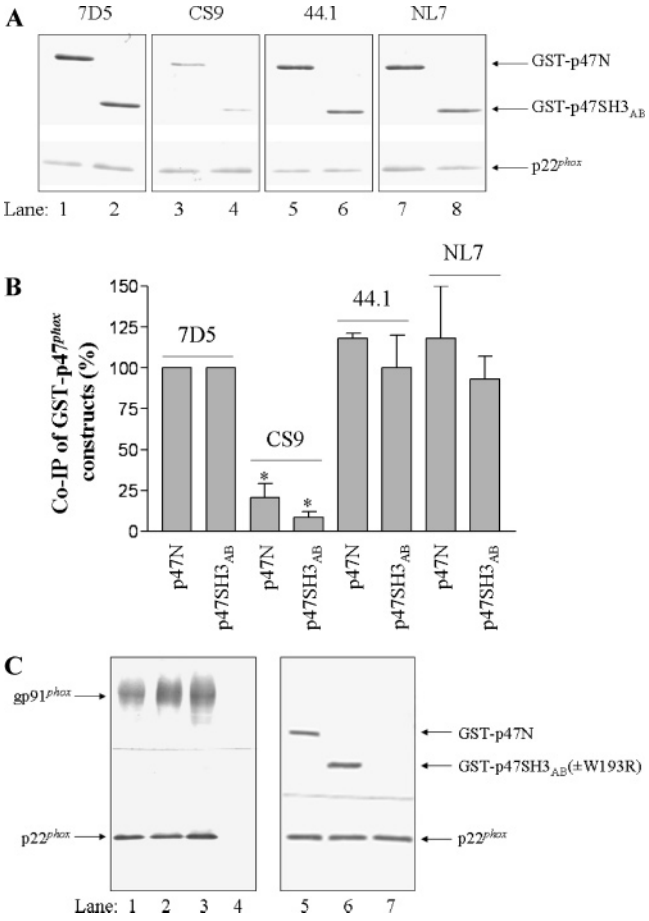

FIGURE 2: Structure analysis of the p47*phox* SH3 domain binding site using Cyt *b*-specific mAbs. Following solubilization of human neutrophil membranes, extracts were incubated with PBS, GST-p47N, or GST-p47SH3$_{AB}$, and Cyt *b* was subsequently immunoprecipitated using a panel of mAb affinity matrices. For immunoblot analysis of eluted bead samples, nitrocellulose membranes were cut in half with the upper panel stained for GST to detect the p47*phox* constructs and the lower panel stained for p22*phox* as a measure of Cyt *b*. (A) Representative co-IP experiment with gel loadings as follows: lane 1, co-IP of GST-p47N with mAb 7D5; lane 2, co-IP of GST-p47SH3$_{AB}$ with mAb 7D5; lane 3, co-IP of GST-p47N with mAb CS9; lane 4, co-IP of GST-p47SH3$_{AB}$ with mAb CS9; lane 5, co-IP of GST-p47N with mAb 44.1; lane 6, co-IP of GST-p47SH3$_{AB}$ with mAb 44.1; lane 7, co-IP of GST-p47N with mAb NL7; lane 8, co-IP of GST-p47SH3$_{AB}$ with mAb NL7. (B) Densitometric analysis of three independent experiments as outlined in part A. To account for variability in staining between experiments, the relative densities were determined for the lanes in individual blots (expressed as GST density/p22*phox* density), with the resulting values normalized to results obtained for mAb 7D5 (set at 100%). In these studies, similar levels of Cyt *b* were immunoprecipitated by each respective affinity matrix in the presence and absence of the p47*phox* constructs. Conditions that showed a significant difference relative to co-IP with mAb 7D5 ($P \leq 0.05$) are labeled with an asterisk. (C) In order to demonstrate the specificity of studies shown in Figures 1 and 2A, a point mutation that disrupts the binding of p47*phox* was introduced in GST-p47SH3$_{AB}$ for binding assays with detergent-solubilized Cyt *b*. Lanes 1−4 show the binding of Cyt *b* by glutathione-Agarose beads loaded with GST-p47SH3$_{AB}$ and GST-p47SH3$_{AB}$(W193R) (as outlined in Figure 1 for GST-p47N) with the gel loadings as follows: lane 1, GST-p47SH3$_{AB}$ supernatant; lane 2, GST-p47SH3$_{AB}$ beads; lane 3, GST-p47SH3$_{AB}$(W193R) supernatant; lane 4, GST-p47SH3$_{AB}$(W193R) beads. Lanes 5−7 of this figure show the co-IP of GST-p47N, GST-p47SH3$_{AB}$, and GST-p47SH3$_{AB}$-(W193R) with Cyt *b* (as outlined in Figure 2A) with the gel loadings as follows: lane 5, co-IP of GST-p47N with mAb 7D5; lane 6, co-IP of GST-p47SH3$_{AB}$ with mAb 7D5; and lane 7, co-IP of GST-p47SH3$_{AB}$(W193R)with mAb 7D5.

peptides retained on the affinity matrix (*55*). Figure 3A shows a representative positive ion MALDI spectrum where the masses observed at 4605.5 and 2303.4 Da could be assigned to the singly and doubly protonated species of p22*phox* residues 149−194 containing the naturally occurring Ala174 polymorphism (*56*). Confidence in this interpretation was provided by the assignment of the singly (4634.7 Da) and doubly (2317.4 Da) protonated species of p22*phox* residues 149−194 containing the naturally occurring Val174 polymorphism (*56*). Importantly, the above polymorphism has been observed in our previous mass analysis of Cyt *b* (*46*), and recent sequence analysis of the mAb CS9 variable domain genes (data not shown) confirms that the observed masses do not correspond to tryptic digest products of the mAb. It is of interest to note that the tryptic peptide bound by mAb CS9 contained missed trypsin cleavage sites at Lys165 and Lys166, which are residues in the core epitope region assigned by phage display analysis and appear to be protected against trypsin digestion in the mAb CS9:Cyt *b* complex.

In order to fine map the mAb CS9 epitope, a synthetic peptide corresponding to residues 161−173 of human p22*phox* (Ac-AEARKKPSEEEAA-coNH_2) was generated and tested for the ability to disrupt the binding of mAb CS9 to Cyt *b*. In IP studies, the peptide Ac-AEARKKPSEEEAA-$CONH_2$ (200 μM final) effectively disrupted the binding of Cyt *b* to mAb CS9-Sepharose (approximately 40−90 nM Cyt *b* and 1733 nM mAb final) (Figure 3B). While a scrambled version of the above peptide was not synthesized due to the extensive epitope characterization that has been provided (refs *43* and *57* and this study), it serves to mention that the irrelevant, mAb 44.1 epitope-mimicking peptide Ac-PQVRPI-$CONH_2$ was examined (200 μM final) and had no measurable effect on the mAb CS9:Cyt *b* interaction (Figure 3B). The studies outlined above assign p22*phox* residues ^{165}KKPSE as the mAb CS9 epitope and allow for confident use of mAb CS9 as a structural probe for Cyt *b*.

Surface Structure Mapping of Reconstituted Cyt b. Although detergent-solubilized Cyt *b* represents a more experimentally tractable sample for most assay systems, results obtained for integral membrane proteins in detergents must be confirmed in the context of more native-like membrane bilayers. In order to generate a more biologically relevant sample, Cyt *b* was extracted from neutrophil membranes, partially purified, and then reconstituted into 99% phosphatidylcholine (PC) membrane vesicles for structure analysis.

In previous studies by our group, the fluorescent probe Cascade Blue (CCB) was conjugated to Cyt *b* binding proteins (wheat germ agglutinin and mAb 44.1), and resonance energy transfer was used to measure binding interactions (*12*, *35*, *43*). Since mAb CS9 was shown to have an overlapping binding site with the p47*phox* SH3 domains (using detergent-solubilized Cyt *b*) in this study, a CCB-CS9 conjugate was generated as a sensitive probe for structure analysis of Cyt *b* in the membrane environment. The feasibility of conducting RET measurements using proteoliposomes as the source of Cyt *b* is shown in Figure 4A, where the fluorescence emission of CCB-CS9 (20 nM CS9 final) was quenched following the addition of reconstituted Cyt *b* (~21−28 nM Cyt *b* final) to the fluorescence cuvette (curves a and c). This observed fluorescence quench-

Table 2: Surface Structure Mapping of Detergent-Solubilized Cyt *b*

	assay system		
probe	pull-down	co-IP	IP
GST-p47N	mAb CS9 disrupts binding of probe to Cyt *b*	−	−
GST-p47SH3$_{AB}$	mAb CS9 disrupts binding of probe to Cyt *b*	−	−
CS9-Sepharose	−	probe disrupts binding of GST-p47N and GST-p47SH3$_{AB}$ to Cyt *b*	mAb 44.1 has no effect on IP of Cyt *b* by the probe
44.1-Sepharose	−	probe has no effect on binding of GST-p47N and GST-p47SH3$_{AB}$ to Cyt *b*	mAb CS9 has no effect on IP of Cyt *b* by the probe
NL7-Sepharose	−	probe has no effect on binding of GST-p47N and GST-p47SH3$_{AB}$ to Cyt *b*	−

ing occurs when CCB fluorophores (donor molecules) are brought into relatively close proximity of the Cyt *b* heme prosthetic groups (acceptor molecules) and provides a measure of the mAb CS9:Cyt *b* binding interaction. The specificity of this binding interaction was demonstrated by

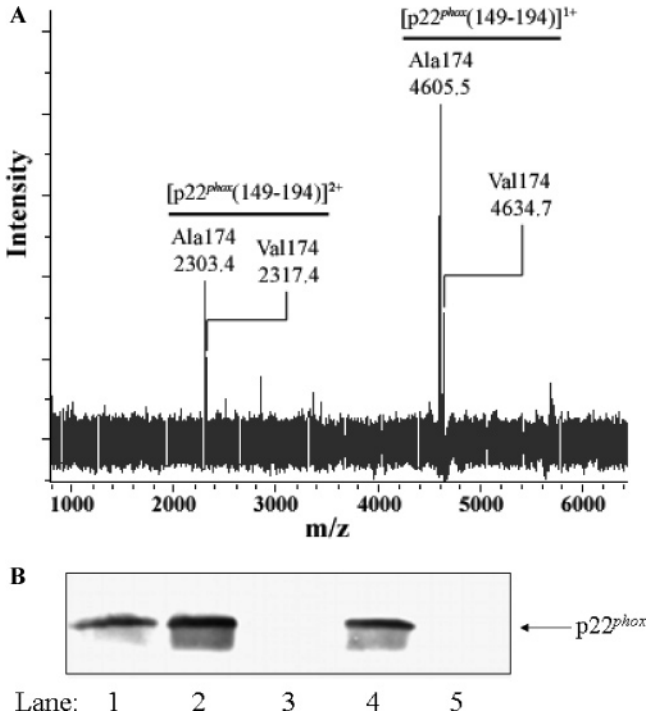

FIGURE 3: Physical mapping of the mAb CS9 binding site on p22^{phox}. (A) MALDI peptide mass mapping was used to characterize the mAb CS9 epitope. Representative positive ion MALDI spectrum following tryptic digestion of purified Cyt *b* bound to mAb CS9-Sepharose beads. The observed masses could be assigned to p22^{phox} residues 149−194 containing the Ala174 or Val174 polymorphism (+1 and +2 charge states) as indicated. Mass accuracies were at least 0.01% for the assigned peaks in this spectrum. (B) For fine mapping, a synthetic peptide corresponding to residues 161−173 of p22^{phox} was generated and analyzed for the ability to disrupt immunoprecipitation of Cyt *b* by mAb-CS9. Lane 1, DDM extract (total Cyt *b*); lane 2, mAb K16-Sepharose (irrelevant mAb) supernatant fraction; lane 3, mAb CS9-Sepharose supernatant fraction; lane 4, mAb CS9-Sepharose supernatant fraction + epitope mimicking peptide Ac-AEARKKPSEEEAA-CONH$_2$; and lane 5, mAb CS9-Sepharose supernatant fraction + irrelevant peptide Ac-PQVRPI-CONH$_2$.

the ability of unlabeled mAb CS9 (390 nM final) and the epitope-mimicking peptide Ac-AEARKKPSEEEAA-CONH$_2$ (200 μM final) to disrupt the CCB-CS9:Cyt *b* interaction as judged by a combination of both RET (Figure 4A, curve b and data not shown) and size exclusion chromatography (Figure 4B, curves a and b and data not shown). In control experiments, unlabeled mAb CS9 (390 nM final) and PC vesicles alone (200 μg/mL final) had no effect on the fluorescence emission of CCB-CS9 (data not shown).

In order to evaluate results obtained in the structure analysis of detergent solubilized Cyt *b*, a combination of RET and size exclusion chromatography was used to examine the ability of Cyt *b*-specific mAbs and the p47^{phox} SH3 domains to disrupt binding of the CCB-CS9 conjugate to reconstituted Cyt *b*. As shown in Figure 4C, D, preincubation of proteoliposomes with GST-p47SH3$_{AB}$ diminished binding of CCB-CS9 to Cyt *b* (20 nM CS9, 630 nM GST-p47SH3$_{AB}$, and ~21−28 nM Cyt *b* final), as judged by the reduction in overall fluorescence quenching relative to the addition of proteoliposomes preincubated with buffer alone (curves a and b). Control experiments demonstrated that preincubation of reconstituted Cyt *b* with GST alone (630 nM final) or GST-p47SH3$_{AB}$(W193R) (630 nM final) had no significant effect on fluorescence quenching and that GST-p47SH3$_{AB}$ (630 nM final) did not effect the emission of CCB-CS9 in the absence of Cyt *b* (Figure 4C, curve c; Figure 4D; and data not shown). Analysis of similar reaction mixtures by size exclusion chromatography confirmed that preincubation of proteoliposomes with GST-p47SH3$_{AB}$ disrupted the binding of the CCB-CS9 conjugate (Figure 4B, curves a and c). This chromatographic data is of fundamental importance for the correct interpretation of RET data, as the decreased fluorescence quenching observed in Figure 4C could result from physical disruption of the CCB-CS9:Cyt *b* binding interaction or from conformational changes in Cyt *b* (*12*, *35*). Since GST-p47N efficiently bound detergent-solubilized Cyt *b* from neutrophil membrane extracts in the present study (Figures 1 and 2), it was of interest to note that anionic lipid (10:0 PA) was required to observe a reduction in the quenching of CCB-CS9 in RET experiments using reconstituted Cyt *b* (Figure 4D). These results are in agreement with previous demonstrations of a partial masking of the tandem SH3 domains in p47N (*58*, *59*) that is relieved by

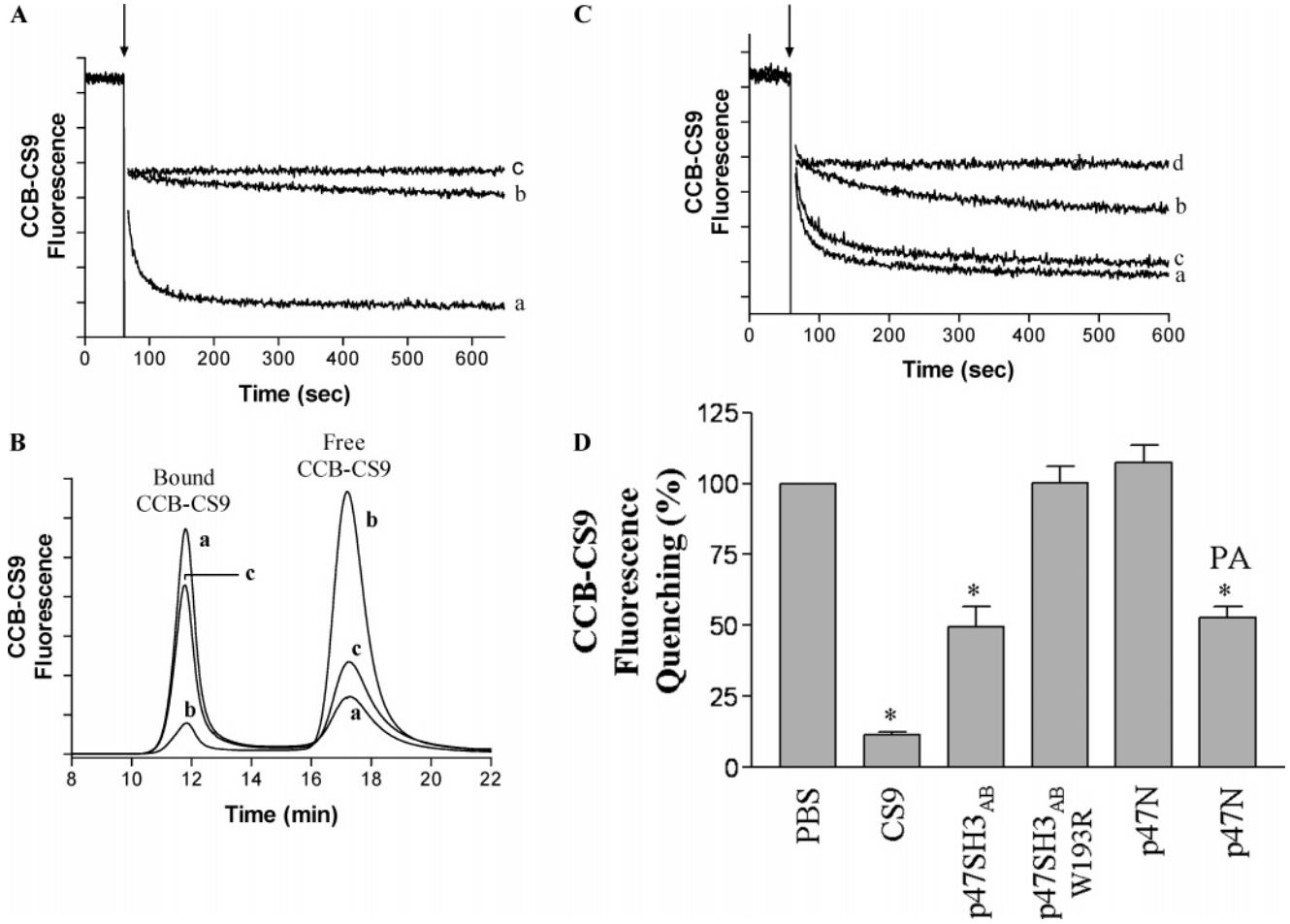

FIGURE 4: Structural overlap of the binding sites for mAb CS9 and the p47^{phox} SH3 domains on reconstituted Cyt *b*. In order to evaluate binding of mAb CS9 to reconstituted Cyt *b*, the fluorescence emission of CCB-CS9 was analyzed by RET and size exclusion chromatography. The ability of mAbs, GST-p47N, and GST-p47SH3$_{AB}$ to disrupt binding of CCB-CS9 to Cyt *b* was determined by preincubation with proteoliposomes prior to analysis. (A) Fluorescence emission of CCB-CS9 following the addition of proteoliposomes that were preincubated with PBS (curve a) or unlabeled mAb CS9 (curve b). Curve c shows the dilution effect observed by addition of samples to the fluorescence cuvette. Crosshatches on the *Y* axis are equal to 15 000 counts/s. (B) Size exclusion profile of CCB-CS9 following addition of reconstituted Cyt *b* that was preincubated with PBS (curve a), unlabeled mAb CS9 (curve b), or GST-p47SH3$_{AB}$ (curve c). Control experiments demonstrated that proteoliposomes eluted in the void volume at ~12 min, while the ~17.5 min peak represents the elution profile of free IgG. Results are representative of at least three chromatographic runs. Crosshatches on the *Y* axis are equal to 100 mV. (C) Same as part A, but following preincubation of reconstituted Cyt *b* with PBS (curve a), GST-p47SH3$_{AB}$ (*curve b*), and GST-p47SH3$_{AB}$(W193R) (curve c). Curve d shows the dilution effect observed by addition of samples to the fluorescence cuvette. Crosshatches on the *Y* axis are equal to 10 000 counts/s. (D) Summary of results for at least three replicates in RET experiments. The effects of agents under investigation on the fluorescence quenching of CCB-CS9 were evaluated by setting the values obtained for PBS incubations as 100% quenching. RET experiments conducted in the presence of 10:0 PA are indicated and conditions that showed a significant difference relative to PBS-treated proteoliposomes ($P \leq 0.05$) are labeled with an asterisk.

arachidonic acid (*47*), and they appear to indicate that the nonionic detergent DDM and/or anionic lipids present in neutrophil membrane extracts alter the structure of p47N.

For a more comprehensive structure analysis of the mAb CS9 binding site on reconstituted Cyt *b*, the binding of CCB-CS9 was analyzed as described above following preincubation of proteoliposomes with mAb 44.1 or mAb NL7 (20 nM CS9, 390 nM mAb 44.1 or NL7, and ~21−28 nM Cyt *b* final). Using both RET and size exclusion chromatography, mAbs NL7 and 44.1 showed no ability to disrupt the binding of CCB-CS9 to reconstituted Cyt *b* (data not shown). The lack of overlap between the mAb 44.1 and CS9 binding sites observed for reconstituted Cyt *b* was an unanticipated finding in light of the close proximity of mAb CS9 and 44.1 core epitope regions on the C-terminal, cytoplasmic domain of p22^{phox} (Table 1). In support of these results, the ability of mAbs 44.1 and CS9 to simultaneously bind the surface of detergent-solubilized Cyt *b* was confirmed in co-IP experiments where mAb 44.1 had no effect on the immunoprecipitation of Cyt *b* by CS9-Sepharose, and mAb CS9 had no effect on the immunoprecipitation of Cyt *b* by 44.1-Sepharose (1733 nM mAb on beads, 1000 nM competing mAb, and ~40−90 nM Cyt *b* final) (data not shown). The results of Cyt *b* structure analysis in both detergent micelles and 99% PC proteoliposomes are summarized in Tables 2 and 3.

Binding of mAb CS9 and the p47^{phox} SH3 Domains Modulates the Structure of Cyt b. Previous reports have demonstrated unique functional effects of both mAb CS9 and p47SH3$_{AB}$ that have yet to be explained including (1) the ability of mAb CS9 to inhibit superoxide production by Cyt *b* supported by a p67^{phox} (1−212)-Rac1 fusion protein (in the complete absence of p47^{phox}) (*43*) and (2) the ability of p47SH3$_{AB}$ to support low levels of superoxide production

Table 3: Analysis of Surface Structure and Conformational Changes Using Reconstituted Cyt *b*

	assay system	
probe	RET	size exclusion
CCB-CS9	$p47SH3_{AB}$ decreases quenching of probe by Cyt *b* in the presence and absence of 10:0 PA	$p47SH3_{AB}$ disrupts binding of probe to Cyt *b*
CCB-CS9	p47N decreases quenching of probe by Cyt *b* in the presence of 10:0 PA	–
CCB-CS9	mAb 44.1 and NL7 have no effect on quenching of probe by Cyt *b*	mAb 44.1 and NL7 do not disrupt binding of probe to Cyt *b*
CCB-44.1	$p47SH3_{AB}$ decreases quenching of probe by Cyt *b*[a]	$p47SH3_{AB}$ does not disrupt binding of probe to Cyt *b*
CCB-44.1	mAb CS9 decreases quenching of probe by Cyt *b*[a]	mAb CS9 does not disrupt binding of probe to Cyt *b*
CCB-44.1	mAb NL7 has no effect on quenching of probe by Cyt *b*	mAb NL7 does not disrupt binding of probe to Cyt *b*

[a] Effect also observed for purified, detergent-solubilized Cyt *b*.

in a recombinant, whole-cell oxidase system (*60*). The observation that mAb CS9 and $p47SH3_{AB}$ bind an overlapping site of the C-terminal region of $p22^{phox}$ raised the possibility that binding of both agents alters the structure of Cyt *b* (with distinct consequences on superoxide generation).

Since results obtained in the present study demonstrated a lack of overlap between the mAb 44.1 epitope and the CS9/$p47SH3_{AB}$ binding sites, CCB-44.1 was used as a probe for both RET and size exclusion chromatography to evaluate the effect of mAb CS9 and $p47SH3_{AB}$ binding on the structure of Cyt *b*. Similar to RET studies with CCB-CS9 (described above), addition of proteoliposomes to CCB-44.1 caused a quenching of fluorescence as a result of binding to Cyt *b* (data not shown). The specificity of this binding interaction was demonstrated by the ability of unlabeled mAb 44.1 to eliminate the quenching observed in RET studies (Figure 5A), with physical disruption of the CCB-44.1:Cyt *b* interaction confirmed by size exclusion chromatography (data not shown). As shown in Figure 5A, a substantial reduction in the overall fluorescence quenching of CCB-44.1 (20 nM 44.1 final) was observed in RET studies following preincubation of Cyt *b*-containing proteoliposomes (~21−28 nM Cyt *b* final) with either mAb CS9 (390 nM final) or GST-$p47SH3_{AB}$ (630 nM final). When similar reaction mixtures were analyzed by size exclusion chromatography, the binding of mAb CS9 and GST-$p47SH3_{AB}$ had no effect on the free CCB-44.1 population (did not physically dissociate the CCB-44.1:Cyt *b* complex) and mediated a reproducible increase in the fluorescence emission of the bound CCB-44.1 (Figure 5B). Taken together, these results indicate that mAb CS9 and GST-$p47SH3_{AB}$ bind reconstituted Cyt *b* simultaneously with CCB-44.1 and reduce the overall fluorescence quenching of the CCB-44.1 population that is bound to Cyt *b*. This relaxation of fluorescence quenching provides evidence that binding of mAb CS9 and the $p47^{phox}$ SH3 domains causes conformational changes in Cyt *b* that increases the distance and/or alters the orientation between the CCB:heme donor:acceptor pair (*61*).

In order to gain additional evidence that binding of the $p47^{phox}$ SH3 domains alters the conformation of Cyt *b*, RET studies were conducted using immunoaffinity-purified Cyt *b*. In these studies, DDM-solubilized Cyt *b* (30 nM final) was preincubated with CCB-44.1 (20 nM 44.1 final) to allow complex formation prior to addition of the agents under investigation. Importantly, the addition of GST-$p47SH3_{AB}$ (200 nM final) to the preformed CCB-44.1:Cyt *b* complex resulted in a substantial relaxation of fluorescence quenching (Figure 6, curve b). A nearly identical relaxation of fluorescence quenching was observed when $p47SH3_{AB}$ (200 nM final) was added to the CCB-44.1:Cyt *b* complex (Figure 6, curve c), demonstrating that the GST portion of the intact fusion protein had no measurable effect on the assay system. In contrast to the above results, the addition of GST-$p47SH3_{AB}$(W193R) (200 nM final) to the preformed CCB-44.1:Cyt *b* complex had no measurable effect on the fluorescence quenching (Figure 6, curve d), consistent with the inability of this mutant to bind Cyt *b*. Since mAb 44.1 and GST-$p47SH3_{AB}$ were shown to simultaneously bind DDM-solubilized Cyt *b* in this study, the observed relaxation of fluorescence quenching cannot be explained by the physical dissociation of the CCB-44.1:Cyt *b* complex and confirms the $p47^{phox}$ SH3 domain-induced conformational changes that were observed for reconstituted Cyt *b*.

$p47^{phox}$ SH3 Domains Enhance Superoxide Production by Cyt b. Although both full length $p47^{phox}$ and p47N have been shown to enhance superoxide production in cell-free assay systems using recombinant $p67^{phox}$ and Rac to activate Cyt *b*, a similar enhancing effect has yet to be described for the $p47^{phox}$ SH3 domains (*20*, *62*). Since the studies outlined above suggested that the $p47^{phox}$ SH3 domains alter the conformation of Cyt *b*, the possibility of a functional

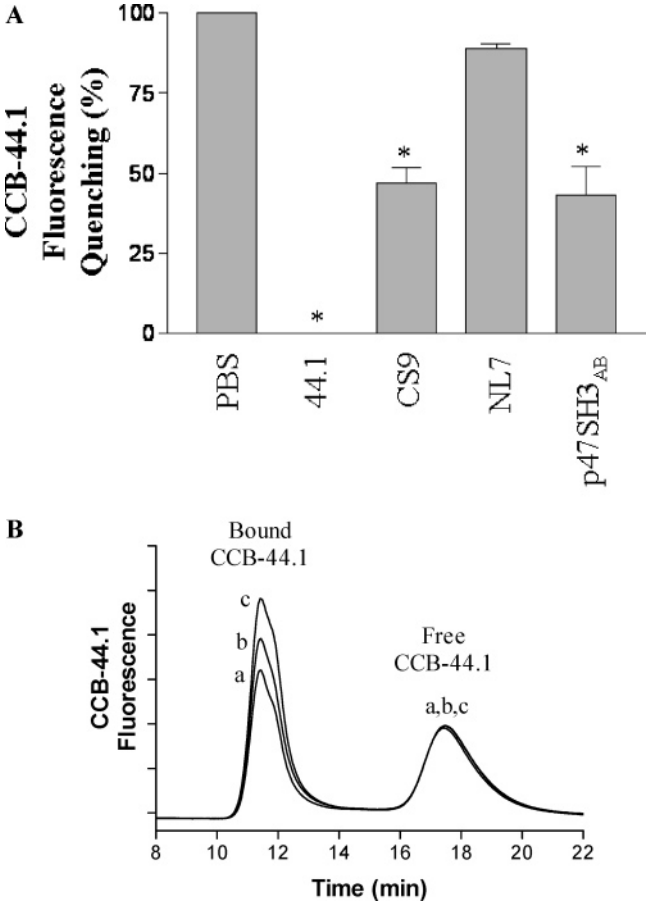

FIGURE 5: Binding of both mAb CS9 and the p47*phox* SH3 domains induces conformational changes in reconstituted Cyt *b*. RET and size exclusion chromatography were used to monitor the effect of Cyt *b*-specific mAbs and GST-p47SH3$_{AB}$ on the fluorescence emission and binding of CCB-44.1 in the presence of reconstituted Cyt *b*. (A) The fluorescence emission of CCB-44.1 was monitored following the addition of reconstituted Cyt *b* (in the presence and absence of unlabeled mAbs and GST-p47SH3$_{AB}$) as outlined in Figure 4A,C. Summary of results for at least three RET experiments, with conditions that showed a significant difference relative to PBS-treated proteoliposomes ($P \leq 0.05$) labeled with an asterisk. (B) In order to examine the effects of mAb CS9 and GST-p47SH3$_{AB}$ on the binding of CCB-44.1, the reaction mixtures used for RET analysis were analyzed by size exclusion chromatography following preincubation of reconstituted Cyt *b* with PBS (curve a), mAb CS9 (curve b), or GST-p47SH3$_{AB}$ (curve c). Results are representative of at least three separate chromatographic profiles. Crosshatches on the *Y* axis are equal to 50 mV.

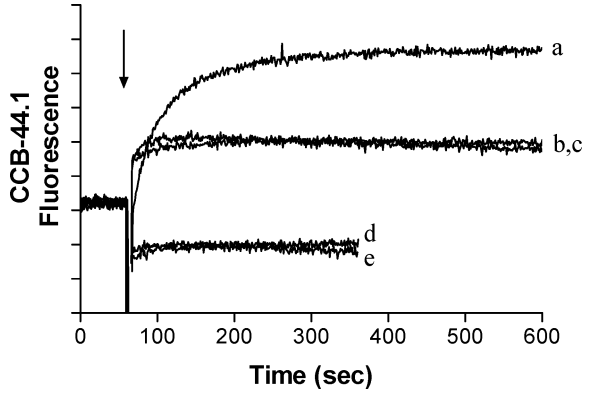

FIGURE 6: Binding of the p47*phox* SH3 domains induces conformational changes in immunoaffinity-purified Cyt *b*. RET analysis was conducted using CCB-44.1 and purified, DDM-solubilized Cyt *b* to examine the effects p47SH3$_{AB}$. Following preincubation of CCB-44.1 with purified Cyt *b*, fluorescence emission of the preformed complex was monitored before and after the addition of the epitope-mimicking peptide Ac-PQVRPI-CONH$_2$ (curve a), GST-p47SH3$_{AB}$ (curve b), p47SH3$_{AB}$ (curve c), and GST-p47SH3$_{AB}$-(W193R) (curve d). The relaxation of fluorescence quenching in curve a provides an estimate of the total quenching in the system due to the binding of CCB-44.1 to Cyt *b*. Curve e shows the dilution effect observed by addition of samples to the fluorescence cuvette and crosshatches on the *Y* axis are equal 10 000 counts/second.

consequence for this interaction was investigated using in vitro superoxide production assays.

As shown in Figure 7A, the presence of p47SH3$_{AB}$ enhanced superoxide production in a cell-free assay system using isolated neutrophil membranes as the source of Cyt *b*, a p67*phox* (1−212)-Rac1(Q61L) fusion protein as the oxidase cytosolic regulatory subunits, and 10:0 PA as the anionic lipid activator. In similar studies with 99% PC reconstituted Cyt *b* (membrane samples used in RET and size exclusion chromatography), the presence of p47SH3$_{AB}$ resulted in an even more pronounced enhancement of superoxide production (Figure 7B). When the concentration dependence of p47N and p47SH3$_{AB}$ were directly compared in cell-free assays, the p47N fragment was notably more effective at enhancing superoxide production at lower concentrations, while the enhancement by p47N and p47SH3$_{AB}$ was similar when both agents were provided at 400 nM in the assay system (data not shown). The specificity of the results described above was supported by the inability of GST-p47SH3$_{AB}$(W193R) to enhance superoxide production in cell-free assays (Figure 7C). In addition to the cell-free assay system described above, similar results were also obtained when GST-p67*phox* (1−212)-Rac1 was used in place of p67*phox* (1−212)-Rac1(Q61L) as the source of oxidase regulatory subunits and when neutrophil membrane dilution vesicles (*63*) were used as the source of Cyt *b* (data not shown). These studies demonstrate a novel functional effect of the interaction of the p47*phox* SH3 domains with Cyt *b* and support a model where p47*phox* alters the conformation of Cyt *b* in a manner that facilitates the activation of superoxide production.

DISCUSSION

In phagocytic leukocytes, binding the regulatory subunit p47*phox* to the integral membrane protein flavocytochrome *b* represents an initial step in assembly of the NADPH oxidase complex and is absolutely required for superoxide production (*64*). A proline rich motif on the C-terminal region of the Cyt *b* subunit p22*phox* provides a critical target for the p47*phox* tandem SH3 domains (*32*, *33*, *65*) following the disruption of p47*phox* autoinhibitory interactions (*14*, *16*, *47*) in activated phagocytes. While binding of p47*phox* and p47*phox* fragments containing the tandem SH3 domains has been extensively studied using peptides containing the proline rich region of p22*phox* (*32*, *33*, *51*, *66*), the interaction of the p47*phox* SH3 domains with the intact Cyt *b* heterodimer remains to be characterized. In the present study, binding of the p47*phox* tandem SH3 domains to Cyt *b* was examined in the context of both detergent micelles and membrane vesicles, with emphasis placed on structure analysis at the level of Cyt *b*.

The Cyt *b*-specific mAb CS9 markedly inhibits superoxide production in an in vitro cell-free assay system (*43*), making this a particularly interesting probe for investigating oxidase

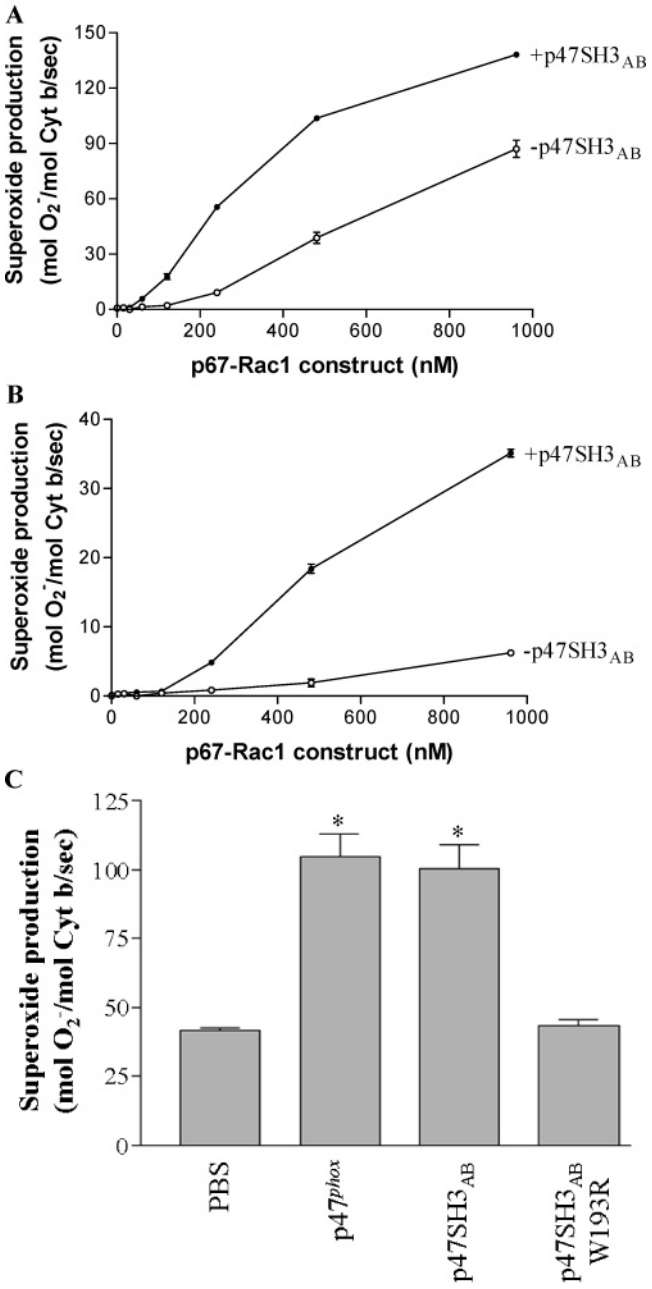

FIGURE 7: Binding of the p47^{phox} SH3 domains enhances superoxide production in a cell-free assay system. In order to evaluate functional effects of the p47^{phox} SH3 domains, a cell-free assay system was used to measure superoxide production using both neutrophil membranes and 99% PC proteoliposomes as sources of Cyt *b*, 10:0 PA as the anionic lipid activator, and a p67^{phox} (1−212)-Rac1(Q61L) fusion protein as the oxidase regulatory subunits. (A) Superoxide production rates of isolated neutrophil membrane fractions in the presence and absence of p47SH3$_{AB}$. (B) Superoxide production rates of 99% PC reconstituted Cyt *b* in the presence and absence of p47SH3$_{AB}$. (C) Superoxide production rates of isolated neutrophil membrane fractions in the presence and absence of GST-p47^{phox}, GST-p47SH3$_{AB}$, and GST-p47SH3$_{AB}$(W193R). Results were obtained from four measurements, and conditions that showed a significant difference relative to PBS-treated neutrophil membranes ($P \leq 0.05$) are labeled with an asterisk.

activation mechanisms. In the present study, multiple lines of evidence demonstrated the ability of mAb CS9 and the p47^{phox} SH3 domains to compete for binding to the cytoplasmic surface of Cyt *b*. To confidently interpret such observations, the mAb CS9 core epitope (previously assigned as ^{165}KKPSE by phage display analysis) (*43*) was directly confirmed in the present study by combination MALDI mass spectrometry and the identification of an epitope-mimicking synthetic peptide. This confident assignment of the mAb CS9 epitope confirms deletion mutagenesis studies of the p22^{phox} subunit (*57*), and it indicates that CS9 and p47SH3$_{AB}$ compete for binding primarily due to the recognition of core binding determinants that are directly adjacent on the C-terminal cytoplasmic tail of p22^{phox}. The ability of mAb CS9 to disrupt binding of the p47^{phox} SH3 domains indicates that this antibody can interfere a critical event in oxidase assembly and provides an explanation for the inhibitory action of CS9 in cell-free assays using neutrophil cytosol as the source of regulatory oxidase subunits (evidence for a more complex inhibitory mechanism is presented below). The potential therapeutic utility of agents that specifically disrupt oxidase assembly is highlighted by studies where cellular delivery of a peptide derived from the first cytoplasmic loop of gp91^{phox} (a predicted binding site for p47^{phox}) (*67*) was shown to attenuate elevated blood pressure in a mouse model of hypertension (*68*). Current efforts are underway to examine the ability of mAb CS9 to inhibit superoxide production in intact cells following the conjugation of protein transduction domains (*69*).

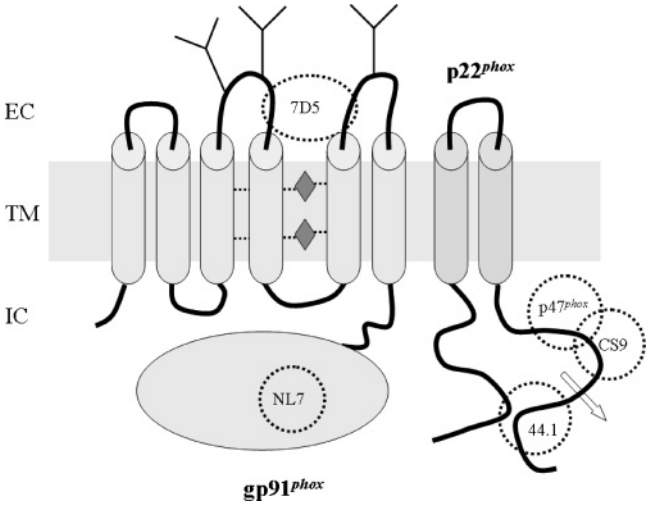

FIGURE 8: Surface structure and conformational dynamics of human neutrophil Cyt *b*. Structural model of Cyt *b* showing the gp91^{phox} and p22^{phox} subunits of the heterodimer, including mapped binding sites for mAb 7D5, mAb CS9, mAb 44.1, mAb NL7, and the p47^{phox} SH3 domains (see Table 1). Structural overlap of the mAb CS9/p47^{phox} SH3 domains is depicted by the overlapping circles, while all other agents examined mapped to distinct regions of both detergent-solubilized and reconstituted Cyt *b*. Arrow at the C-terminal tail of p22^{phox} represents Cyt *b* conformational changes induced by anionic lipids, mAb CS9 and p47SH3$_{AB}$ that have been detected using CCB-44.1 as a structural probe. EC, extracellular; TM, transmembrane; IC, intracellular.

Since Cyt *b* is a relatively low abundance integral membrane protein that contains notable structural heterogeneity (extensive glycosylation of the gp91^{phox} subunit and polymorphic variants in the p22^{phox} subunit) (*46*), difficulties exist in economically obtaining adequate levels of purified material for structure determination. In light of this situation, sensitive biochemical methods remain critical for advancing Cyt *b* structure models. In the present study, biochemical analysis of both detergent-solubilized and reconstituted Cyt *b* indicated a lack of overlap between (1) the mAb 44.1

epitope and the CS9/p47^{phox} SH3 domain binding sites on Cyt *b* and (2) the mAb NL7 epitope and the mAb 44.1, mAb CS9, and p47^{phox} SH3 domain binding sites on Cyt *b*. The results obtained for mAb NL7 confirm previous studies that indicated a lack of overlap between the mAb NL7 and 44.1 epitopes on detergent-solubilized Cyt *b* (*43*) and extend this finding to a larger segment of the p22^{phox} C-terminal domain. Further studies are required to determine the mechanism by which mAb NL7 inhibits superoxide production by the NADPH oxidase (*44*). The ability of mAb 44.1 to simultaneously bind Cyt *b* with CS9 or the p47^{phox} tandem SH3 domains in the present study is of interest in light of the close proximity of each core binding site on the C-terminal region of p22^{phox}. Importantly, this observation was supported by distinct methods analyzing both detergent-solubilized and functionally reconstituted Cyt *b*. In order to eliminate steric hindrance between two relatively large binding partners, it would seem necessary that p22^{phox} residues 170−181 (which separate the core mAb CS9 and 44.1 epitopes) adopt an extended conformation and/or contain a structural motif that provides a distinct orientation of binding partners on the surface of Cyt *b*. Inspection of the p22^{phox} primary sequence reveals the sequence ^{177}GGPPGG, which is notable since Pro and Gly residues are known to reside preferentially in turn and random coil regions of protein structures (*70*, *71*). In a previous study by our group using RET, mAb CS9 was shown to cause a substantial relaxation in fluorescence quenching when added to a detergent-solubilized CCB-44.1:Cyt *b* complex (*43*), which was incorrectly interpreted to indicate a physical disruption of the CCB-44.1:Cyt *b* complex due to overlap of the mAb epitopes. Since mAbs 44.1 and CS9 were shown to simultaneously bind Cyt *b* in the present study, the ability of mAb CS9 to diminish fluorescence quenching of the CCB-44.1:Cyt *b* complex (ref *43* and this study) can now be interpreted to represent CS9-induced conformational changes in Cyt *b*. Since mAb CS9 was previously shown to cause a marked inhibition of superoxide production by Cyt *b* when a p67^{phox}(1−212)-Rac1 fusion protein was used as the sole source of oxidase regulatory subunits (*43*), it is interesting to speculate that mAb CS9 locks Cyt *b* in a conformation that inhibits catalytic activity (although structural overlap between the mAb CS9/Rac1-p67^{phox} (1−212) binding sites represents an equally viable alternative) (*72*). It is important to state that the detection of mAb CS9-induced structural changes in Cyt *b* highlights the need to consider potential effects of the structural probe itself in studies of this nature.

Although the p47^{phox} subunit is absolutely required for oxidase activation in phagocytic cells (*64*), the structural consequences of the p47^{phox}:Cyt *b* interaction have yet to be determined. Using CCB-44.1 as a probe for RET and size exclusion chromatography, evidence was obtained in this study consistent with p47SH3$_{AB}$-induced structural changes in Cyt *b*. To this point, RET studies have demonstrated that anionic lipids, the binding of mAb CS9, and the binding of the p47SH3$_{AB}$ all induce conformational changes in Cyt *b* that have been detected at the mAb 44.1 epitope (refs *12* and *43* and this study). The specificity of the above agents for mediating Cyt *b* conformational changes is highlighted by the fact that neutral lipids and other Cyt *b*-specific mAbs (NS5, 54.1, NL7) do not mediate conformational changes that can be detected at the mAb 44.1 epitope (*12*, *43*). While the above data suggests the C-terminal domain of p22^{phox} to contain some degree of structural plasticity, it is important to highlight that the 25 C-terminal residues of this subunit were shown to be dispensable for superoxide production in a heterologous expression system (*57*). If the anionic lipid and p47SH3$_{AB}$-mediated conformational changes that have been observed in our RET studies genuinely play a role in the regulation of superoxide production, such structural changes are likely more global in nature and not restricted to the extreme C-terminus of p22^{phox}.

While the p47^{phox} subunit has been considered primarily an adaptor protein that bridges interactions between Cyt *b* and p67^{phox} (*60*), the possibility exists that p47^{phox} binding has a more complex role in oxidase activation. Such a hypothesis was supported by the unexpected ability of p47SH3$_{AB}$ to enhance superoxide production by p67^{phox} (1−212)-Rac1 fusion proteins in cell-free assays using both neutrophil membranes and 99% PC proteoliposomes as the source of Cyt *b*. Since the p47SH3$_{AB}$ fragment has not been shown to directly bind either Rac1 or p67^{phox} (1−212) to our knowledge, the results obtained in this study are consistent with a model where binding of the p47^{phox} SH3 domains to the proline rich region of p22^{phox} induces conformational changes in Cyt *b* (detected in RET studies) that are important for oxidase activation. Studies in a heterologous expression system previously showed that the p47^{phox} SH3 domains promoted translocation of p67^{phox} and the p67^{phox} N-terminal Rac-binding domain to the membrane (*60*), which may indicate that p47SH3$_{AB}$-mediated conformational changes in Cyt *b* increase the binding affinity for Rac and/or p67^{phox}. In light of the p47SH3$_{AB}$-mediated enhancement of superoxide production reported in the present study, it should be noted that GST-p47SH3$_{AB}$ was previously shown to inhibit superoxide production in cell-free assays using neutrophil cytosol as the source of oxidase regulatory subunits (*33*); an interesting result that likely stemmed from an inhibitory effect on assembly of the p40^{phox}−p47^{phox}−p67^{phox} ternary complex with Cyt *b*. In summary, the present work continues our efforts to characterize the structure of human neutrophil Cyt *b*, and it provides evidence that the regulatory subunit p47^{phox} modulates the conformation of Cyt *b* to facilitate the activation of superoxide production.

ACKNOWLEDGMENT

We gratefully acknowledge the assistance of Dr. Rachel Neal with the mass spectrometry studies, Marcus Kincade for advice concerning peptide synthesis, and the Murdock Charitable Trust for their generous support of the Montana State University Mass Spectrometry Facility.

REFERENCES

1. Elsbach, P., Weiss, J., and Levy, O. (1999) Oxygen-Independent Antimicrobial Systems of Phagocytes, in *Inflammation: Basic Principles and Clinical Correlates* (Gallin, J. I., and Snyderman, R., Eds.) 3rd ed., pp 801−817, Lippincott Williams & Wilkins, Philadelphia.
2. Klebanov, S. J. (1999) Oxygen Metabolites from Phagocytes, in *Inflammation: Basic Principles and Clinical Correlates* (Gallin, J. I., and Snyderman, R., Eds.) 3rd ed., pp 721−768, Lippincott Williams & Wilkins, Philadelphia.
3. Nauseef, W. M. (2004) Assembly of the phagocyte NADPH oxidase, *Histochem. Cell Biol. 122*, 277−291.
4. Cathcart, M. K., Morel, D. W., and Chisolm, G. M., III (1985) Monocytes and neutrophils oxidize low density lipoprotein making it cytotoxic, *J. Leukoc. Biol. 38*, 341−350.

5. Kristal, B., Shurtz-Swirski, R., Chezar, J., Manaster, J., Levy, R., Shapiro, G., Weissman, I., Shasha, S. M., and Sela, S. (1998) Participation of peripheral polymorphonuclear leukocytes in the oxidative stress and inflammation in patients with essential hypertension. *Am. J. Hypertens. 11*, 921−928.
6. Duilio, C., Ambrosio, G., Kuppusamy, P., DiPaula, A., Becker, L. C., and Zweier, J. L. (2001) Neutrophils are primary source of O2 radicals during reperfusion after prolonged myocardial ischemia, *Am. J. Physiol Heart Circ. Physiol 280*, H2649−H2657.
7. Parkos, C. A., Allen, R. A., Cochrane, C. G., and Jesaitis, A. J. (1987) Purified cytochrome b from human granulocyte plasma membrane is comprised of two polypeptides with relative molecular weights of 91,000 and 22,000. *J. Clin. Invest 80*, 732−742.
8. Rotrosen, D., Yeung, C. L., Leto, T. L., Malech, H. L., and Kwong, C. H. (1992) Cytochrome b558: the flavin-binding component of the phagocyte NADPH oxidase, *Science 256*, 1459−1462.
9. Lapouge, K., Smith, S. J., Groemping, Y., and Rittinger, K. (2002) Architecture of the p40−p47−p67phox complex in the resting state of the NADPH oxidase. A central role for p67phox, *J. Biol. Chem. 277*, 10121−10128.
10. Quinn, M. T., Evans, T., Loetterle, L. R., Jesaitis, A. J., and Bokoch, G. M. (1993) Translocation of Rac correlates with NADPH oxidase activation. Evidence for equimolar translocation of oxidase components, *J. Biol. Chem. 268*, 20983−20987.
11. Regier, D. S., Waite, K. A., Wallin, R., and McPhail, L. C. (1999) A phosphatidic acid-activated protein kinase and conventional protein kinase C isoforms phosphorylate p22(phox), an NADPH oxidase component, *J. Biol. Chem. 274*, 36601−36608.
12. Taylor, R. M., Foubert, T. R., Burritt, J. B., Baniulis, D., McPhail, L. C., and Jesaitis, A. J. (2004) Anionic amphiphile and phospholipid-induced conformational changes in human neutrophil flavocytochrome b observed by fluorescence resonance energy transfer, *Biochim. Biophys. Acta 1663*, 201−213.
13. Forbes, L. V., Moss, S. J., and Segal, A. W. (1999) Phosphorylation of p67phox in the neutrophil occurs in the cytosol and is independent of p47phox, *FEBS Lett. 449*, 225−229.
14. Huang, J., and Kleinberg, M. E. (1999) Activation of the phagocyte NADPH oxidase protein p47(phox). Phosphorylation controls SH3 domain-dependent binding to p22(phox), *J. Biol. Chem. 274*, 19731−19737.
15. Someya, A., Nunoi, H., Hasebe, T., and Nagaoka, I. (1999) Phosphorylation of p40-phox during activation of neutrophil NADPH oxidase, *J. Leukoc. Biol. 66*, 851−857.
16. Swain, S. D., Helgerson, S. L., Davis, A. R., Nelson, L. K., and Quinn, M. T. (1997) Analysis of activation-induced conformational changes in p47phox using tryptophan fluorescence spectroscopy, *J. Biol. Chem. 272*, 29502−29510.
17. Diebold, B. A., and Bokoch, G. M. (2001) Molecular basis for Rac2 regulation of phagocyte NADPH oxidase, *Nat. Immunol. 2*, 211−215.
18. Ebisu, K., Nagasawa, T., Watanabe, K., Kakinuma, K., Miyano, K., and Tamura, M. (2001) Fused p47phox and p67phox truncations efficiently reconstitute NADPH oxidase with higher activity and stability than the individual components, *J. Biol. Chem. 276*, 24498−24505.
19. Han, C. H., Freeman, J. L., Lee, T., Motalebi, S. A., and Lambeth, J. D. (1998) Regulation of the neutrophil respiratory burst oxidase. Identification of an activation domain in p67(phox), *J. Biol. Chem. 273*, 16663−16668.
20. Hata, K., Ito, T., Takeshige, K., and Sumimoto, H. (1998) Anionic amphiphile-independent activation of the phagocyte NADPH oxidase in a cell-free system by p47phox and p67phox, both in C terminally truncated forms. Implication for regulatory Src homology 3 domain-mediated interactions, *J. Biol. Chem. 273*, 4232−4236.
21. Sarfstein, R., Gorzalczany, Y., Mizrahi, A., Berdichevsky, Y., Molshanski-Mor, S., Weinbaum, C., Hirshberg, M., Dagher, M. C., and Pick, E. (2004) Dual role of Rac in the assembly of NADPH oxidase, tethering to the membrane and activation of p67phox: a study based on mutagenesis of p67phox-Rac1 chimeras, *J. Biol. Chem. 279*, 16007−16016.
22. Quinn, M. T., Parkos, C. A., Walker, L., Orkin, S. H., Dinauer, M. C., and Jesaitis, A. J. (1989) Association of a Ras-related protein with cytochrome b of human neutrophils, *Nature 342*, 198−200.
23. Berthier, S., Paclet, M. H., Lerouge, S., Roux, F., Vergnaud, S., Coleman, A. W., and Morel, F. (2003) Changing the conformation state of cytochrome b558 initiates NADPH oxidase activation: MRP8/MRP14 regulation, *J. Biol. Chem. 278*, 25499−25508.
24. Martyn, K. D., Kim, M. J., Quinn, M. T., Dinauer, M. C., and Knaus, U. G. (2005) p21-activated kinase (Pak) regulates NADPH oxidase activation in human neutrophils, *Blood 106*, 3962−3969.
25. Guichard, C., Pedruzzi, E., Dewas, C., Fay, M., Pouzet, C., Bens, M., Vandewalle, A., Ogier-Denis, E., Gougerot-Pocidalo, M. A., and Elbim, C. (2005) Interleukin-8-induced priming of neutrophil oxidative burst requires sequential recruitment of NADPH oxidase components into lipid rafts, *J. Biol. Chem. 280*, 37021−37032.
26. Jesaitis, A. J. (1992) Signal transduction in neutrophil membrane domains, *Comments Mol. Cell. Biophys. 8*, 97−114.
27. Quinn, M. T., Parkos, C. A., and Jesaitis, A. J. (1989) The lateral organization of components of the membrane skeleton and superoxide generation in the plasma membrane of stimulated human neutrophils, *Biochim. Biophys. Acta. 987*, 83−94.
28. Biberstine-Kinkade, K. J., DeLeo, F. R., Epstein, R. I., LeRoy, B. A., Nauseef, W. M., and Dinauer, M. C. (2001) Heme-ligating histidines in flavocytochrome b(558): identification of specific histidines in gp91(phox), *J. Biol. Chem. 276*, 31105−31112.
29. Doussiere, J., Buzenet, G., and Vignais, P. V. (1995) Photoaffinity labeling and photoinactivation of the O2(-)-generating oxidase of neutrophils by an azido derivative of FAD, *Biochemistry 34*, 1760−1770.
30. Ravel, P., and Lederer, F. (1993) Affinity-labeling of an NADPH-binding site on the heavy subunit of flavocytochrome b558 in particulate NADPH oxidase from activated human neutrophils, *Biochem. Biophys. Res. Commun. 196*, 543−552.
31. Dinauer, M. C., Pierce, E. A., Erickson, R. W., Muhlebach, T. J., Messner, H., Orkin, S. H., Seger, R. A., and Curnutte, J. T. (1991) Point mutation in the cytoplasmic domain of the neutrophil p22-phox cytochrome b subunit is associated with a nonfunctional NADPH oxidase and chronic granulomatous disease, *Proc. Natl. Acad. Sci. U.S.A. 88*, 11231−11235.
32. Leto, T. L., Adams, A. G., and de Mendez, I. (1994) Assembly of the phagocyte NADPH oxidase: binding of Src homology 3 domains to proline-rich targets, *Proc. Natl. Acad. Sci. U.S.A. 91*, 10650−10654.
33. Sumimoto, H., Kage, Y., Nunoi, H., Sasaki, H., Nose, T., Fukumaki, Y., Ohno, M., Minakami, S., and Takeshige, K. (1994) Role of Src homology 3 domains in assembly and activation of the phagocyte NADPH oxidase. *Proc. Natl. Acad. Sci. U.S.A. 91*, 5345−5349.
34. Doussiere, J., Gaillard, J., and Vignais, P. V. (1996) Electron transfer across the O2- generating flavocytochrome b of neutrophils. Evidence for a transition from a low-spin state to a high-spin state of the heme iron component, *Biochemistry 35*, 13400−13410.
35. Foubert, T. R., Burritt, J. B., Taylor, R. M., and Jesaitis, A. J. (2002) Structural changes are induced in human neutrophil cytochrome b by NADPH oxidase activators, LDS, SDS, and arachidonate: intermolecular resonance energy transfer between trisulfopyrenyl-wheat germ agglutinin and cytochrome b(558), *Biochim. Biophys. Acta 1567*, 221−231.
36. Bauldry, S. A., Bass, D. A., Cousart, S. L., and McCall, C. E. (1991) Tumor necrosis factor alpha priming of phospholipase D in human neutrophils. Correlation between phosphatidic acid production and superoxide generation, *J. Biol. Chem. 266*, 4173−4179.
37. Dana, R., Leto, T. L., Malech, H. L., and Levy, R. (1998) Essential requirement of cytosolic phospholipase A2 for activation of the phagocyte NADPH oxidase, *J. Biol. Chem. 273*, 441−445.
38. Dang, P. M., Cross, A. R., and Babior, B. M. (2001) Assembly of the neutrophil respiratory burst oxidase: a direct interaction between p67PHOX and cytochrome b558, *Proc. Natl. Acad. Sci. U.S.A. 98*, 3001−3005.
39. Paclet, M. H., Coleman, A. W., Vergnaud, S., and Morel, F. (2000) p67-phox-mediated NADPH oxidase assembly: imaging of cytochrome b558 liposomes by atomic force microscopy, *Biochemistry 39*, 9302−9310.
40. Burritt, J. B., Quinn, M. T., Jutila, M. A., Bond, C. W., and Jesaitis, A. J. (1995) Topological mapping of neutrophil cytochrome b epitopes with phage-display libraries, *J. Biol. Chem. 270*, 16974−16980.
41. Burritt, J. B., Busse, S. C., Gizachew, D., Siemsen, D. W., Quinn, M. T., Bond, C. W., Dratz, E. A., and Jesaitis, A. J. (1998) Antibody imprint of a membrane protein surface. Phagocyte flavocytochrome b, *J. Biol. Chem. 273*, 24847−24852.

42. Campion, Y., Paclet, M. H., Jesaitis, A. J., Marques, B., Grichine, A., Berthier, S., Lenormand, J. L., Lardy, B., Stasia, M. J., and Morel, F. (2007) New insights into the membrane topology of the phagocyte NADPH oxidase: Characterization of an anti-gp91-phox conformational monoclonal antibody, *Biochimie 89*, 1145−1158.
43. Taylor, R. M., Burritt, J. B., Baniulis, D., Foubert, T. R., Lord, C. I., Dinauer, M. C., Parkos, C. A., and Jesaitis, A. J. (2004) Site-specific inhibitors of NADPH oxidase activity and structural probes of flavocytochrome b: characterization of six monoclonal antibodies to the p22phox subunit, *J. Immunol. 173*, 7349−7357.
44. Burritt, J. B., Foubert, T. R., Baniulis, D., Lord, C. I., Taylor, R. M., Mills, J. S., Baughan, T. D., Roos, D., Parkos, C. A., and Jesaitis, A. J. (2003) Functional epitope on human neutrophil flavocytochrome b558, *J. Immunol. 170*, 6082−6089.
45. Taylor, R. M., Burritt, J. B., Foubert, T. R., Snodgrass, M. A., Stone, K. C., Baniulis, D., Gripentrog, J. M., Lord, C., and Jesaitis, A. J. (2003) Single-step immunoaffinity purification and characterization of dodecylmaltoside-solubilized human neutrophil flavocytochrome b, *Biochim. Biophys. Acta 1612*, 65−75.
46. Taylor, R. M., Baniulis, D., Burritt, J. B., Gripentrog, J. M., Lord, C. I., Riesselman, M. H., Maaty, W. S., Bothner, B. P., Angel, T. E., Dratz, E. A., Linton, G. F., Malech, H. L., and Jesaitis, A. J. (2006) Analysis of human phagocyte flavocytochrome b(558) by mass spectrometry, *J. Biol. Chem. 281*, 37045−37056.
47. Shiose, A., and Sumimoto, H. (2000) Arachidonic acid and phosphorylation synergistically induce a conformational change of p47phox to activate the phagocyte NADPH oxidase, *J. Biol. Chem. 275*, 13793−13801.
48. Alloul, N., Gorzalczany, Y., Itan, M., Sigal, N., and Pick, E. (2001) Activation of the superoxide-generating NADPH oxidase by chimeric proteins consisting of segments of the cytosolic component p67(phox) and the small GTPase Rac1, *Biochemistry 40*, 14557−14566.
49. Knoller, S., Shpungin, S., and Pick, E. (1991) The membrane-associated component of the amphiphile-activated, cytosol-dependent superoxide-forming NADPH oxidase of macrophages is identical to cytochrome b559, *J. Biol. Chem. 266*, 2795−2804.
50. Lundahl, P., Zeng, C. M., Lagerquist, H. C., Gottschalk, I., and Greijer, E. (1999) Chromatographic approaches to liposomes, proteoliposomes and biomembrane vesicles, *J. Chromatogr. B Biomed. Sci. Appl. 722*, 103−120.
51. Groemping, Y., Lapouge, K., Smerdon, S. J., and Rittinger, K. (2003) Molecular basis of phosphorylation-induced activation of the NADPH oxidase, *Cell 113*, 343−355.
52. Ogura, K., Nobuhisa, I., Yuzawa, S., Takeya, R., Torikai, S., Saikawa, K., Sumimoto, H., and Inagaki, F. (2006) NMR solution structure of the tandem Src homology 3 domains of p47phox complexed with a p22phox-derived proline-rich peptide, *J. Biol. Chem. 281*, 3660−3668.
53. Burritt, J. B., DeLeo, F. R., McDonald, C. L., Prigge, J. R., Dinauer, M. C., Nakamura, M., Nauseef, W. M., and Jesaitis, A. J. (2001) Phage display epitope mapping of human neutrophil flavocytochrome b558. Identification of two juxtaposed extracellular domains, *J. Biol. Chem. 276*, 2053−2061.
54. de Mendez, I., Homayounpour, N., and Leto, T. L. (1997) Specificity of p47phox SH3 domain interactions in NADPH oxidase assembly and activation, *Mol. Cell Biol. 17*, 2177−2185.
55. Parker, C. E., and Tomer, K. B. (2002) MALDI/MS-based epitope mapping of antigens bound to immobilized antibodies, *Mol. Biotechnol. 20*, 49−62.
56. Rae, J., Noack, D., Heyworth, P. G., Ellis, B. A., Curnutte, J. T., and Cross, A. R. (2000) Molecular analysis of 9 new families with chronic granulomatous disease caused by mutations in CYBA, the gene encoding p22(phox), *Blood 96*, 1106−1112.
57. Zhu, Y., Marchal, C. C., Casbon, A. J., Stull, N., von, L. K., Knaus, U. G., Jesaitis, A. J., McCormick, S., Nauseef, W. M., and Dinauer, M. C. (2006) Deletion mutagenesis of p22phox subunit of flavocytochrome b558: identification of regions critical for gp91phox maturation and NADPH oxidase activity, *J. Biol. Chem. 281*, 30336−30346.
58. Hiroaki, H., Ago, T., Ito, T., Sumimoto, H., and Kohda, D. (2001) Solution structure of the PX domain, a target of the SH3 domain, *Nat. Struct. Biol. 8*, 526−530.
59. Karathanassis, D., Stahelin, R. V., Bravo, J., Perisic, O., Pacold, C. M., Cho, W., and Williams, R. L. (2002) Binding of the PX domain of p47(phox) to phosphatidylinositol 3,4-bisphosphate and phosphatidic acid is masked by an intramolecular interaction, *EMBO J. 21*, 5057−5068.
60. de Mendez, I., Adams, A. G., Sokolic, R. A., Malech, H. L., and Leto, T. L. (1996) Multiple SH3 domain interactions regulate NADPH oxidase assembly in whole cells, *EMBO J. 15*, 1211−1220.
61. dos Remedios, C. G., and Moens, P. D. (1995) Fluorescence resonance energy transfer spectroscopy is a reliable "ruler" for measuring structural changes in proteins. Dispelling the problem of the unknown orientation factor, *J. Struct. Biol. 115*, 175−185.
62. Nagasawa, T., Ebisu, K., Inoue, Y., Miyano, K., and Tamura, M. (2003) A new role of Pro-73 of p47phox in the activation of neutrophil NADPH oxidase, *Arch. Biochem. Biophys. 416*, 92−100.
63. Shpungin, S., Dotan, I., Abo, A., and Pick, E. (1989) Activation of the superoxide forming NADPH oxidase in a cell-free system by sodium dodecyl sulfate. Absolute lipid dependence of the solubilized enzyme, *J. Biol. Chem. 264*, 9195−9203.
64. Volpp, B. D., Nauseef, W. M., and Clark, R. A. (1988) Two cytosolic neutrophil oxidase components absent in autosomal chronic granulomatous disease, *Science 242*, 1295−1297.
65. Leusen, J. H., Bolscher, B. G., Hilarius, P. M., Weening, R. S., Kaulfersch, W., Seger, R. A., Roos, D., and Verhoeven, A. J. (1994) 156Pro→Gln substitution in the light chain of cytochrome b558 of the human NADPH oxidase (p22-phox) leads to defective translocation of the cytosolic proteins p47-phox and p67-phox, *J. Exp. Med. 180*, 2329−2334.
66. Nobuhisa, I., Takeya, R., Ogura, K., Ueno, N., Kohda, D., Inagaki, F., and Sumimoto, H. (2006) Activation of the superoxide-producing phagocyte NADPH oxidase requires co-operation between the tandem SH3 domains of p47phox in recognition of a polyproline type II helix and an adjacent alpha-helix of p22phox, *Biochem. J. 396*, 183−192.
67. DeLeo, F. R., Yu, L., Burritt, J. B., Loetterle, L. R., Bond, C. W., Jesaitis, A. J., and Quinn, M. T. (1995) Mapping sites of interaction of p47-phox and flavocytochrome b with random-sequence peptide phage display libraries, *Proc. Natl. Acad. Sci. U.S.A. 92*, 7110−7114.
68. Rey, F. E., Cifuentes, M. E., Kiarash, A., Quinn, M. T., and Pagano, P. J. (2001) Novel competitive inhibitor of NAD(P)H oxidase assembly attenuates vascular O(2)(−) and systolic blood pressure in mice, *Circ. Res. 89*, 408−414.
69. Fischer, P. M., Krausz, E., and Lane, D. P. (2001) Cellular delivery of impermeable effector molecules in the form of conjugates with peptides capable of mediating membrane translocation, *Bioconjug. Chem. 12*, 825−841.
70. Chou, P. Y., and Fasman, G. D. (1974) Conformational parameters for amino acids in helical, beta-sheet, and random coil regions calculated from proteins, *Biochemistry 13*, 211−222.
71. Krieger, F., Moglich, A., and Kiefhaber, T. (2005) Effect of proline and glycine residues on dynamics and barriers of loop formation in polypeptide chains, *J. Am. Chem. Soc. 127*, 3346−3352.
72. Dahan, I., Issaeva, I., Gorzalczany, Y., Sigal, N., Hirshberg, M., and Pick, E. (2002) Mapping of functional domains in the p22-(phox) subunit of flavocytochrome b(559) participating in the assembly of the NADPH oxidase complex by "peptide walking", *J. Biol. Chem. 277*, 8421−8432.

BI701626P